Quantifying Fractional Ground Cover on the Climate Sensitive High Plains Using AVIRIS and Landsat TM Data

By Amanda Susan Warner (M.S., Geology)
Thesis directed by Professor Alexander F.H. Goetz

Abstract

The High Plains is an economically important and climatologically sensitive region of the United States and Canada. The High Plains contain 100,000 sq km of Holocene sand dunes and sand sheets that are currently stabilized by natural vegetation. Droughts and the larger threat of global warming are climate phenomena that could cause depletion of natural vegetation and make this region susceptible to sand dune reactivation. This thesis is part of a larger study that is assessing the effect of climate variability on the natural vegetation that covers the High Plains using Landsat 5 and Landsat 7 data. The question this thesis addresses is how can fractional vegetation cover be mapped with the Landsat instruments using linear spectral mixture analysis and to what accuracy. The method discussed in this thesis made use of a high spatial and spectral resolution sensor called AVIRIS (Airborne Visible and Infrared Imaging Spectrometer) and field measurements to test vegetation mapping in three Landsat 7 sub-scenes.

Near-simultaneous AVIRIS images near Ft. Morgan, Colorado and near Logan, New Mexico were acquired on July 10, 1999 and September 30, 1999, respectively. The AVIRIS flights preceded Landsat 7 overpasses by approximately one hour. These data provided the opportunity to test spectral mixture algorithms with AVIRIS and to use these data to constrain the multispectral mixed pixels of Landsat 7. The comparisons of mixture analysis between the two instruments showed that AVIRIS endmembers can be used to unmix Landsat 7 data with good estimates of soil cover, and reasonable estimates of non-photosynthetic vegetation and green vegetation. Landsat 7 derived image endmembers correlate with AVIRIS fractions, but the error is relatively large and does not give a precise estimate of cover.

Table of Contents

Abstract.....iii
Acknowledgements.....v
Chapter 1: Introduction.....1

Chapter 2:Background.....8

Instrumentation..... 8
Spectral Mixture Analysis Theory..... 9
Spectral Mixture Analysis and Vegetation Mapping..... 11
Dune Stabilization..... 14
Spatial Characteristics..... 15
BRDF..... 16
Physical and Climate Settings..... 19

Chapter 3:Methods.....21

Vegetation Measurements..... 21
Spectral Characterization Procedure..... 24
Atmospheric Correction and Calibration..... 26
Geometric Correction..... 30
Endmember Selection..... 34
Endmember Bundle Variability..... 41
Linear Spectral Unmixing..... 42
Detailed Description of AutoSMA..... 45

Chapter 4: Results.....49

Spectral Characterization..... 49
Unmixing Results, Ft. Morgan..... 51
Combination of FM0209 and FM0210 Endmember Bundles. 62
Logan, NM..... 65

Chapter 5: Discussion and Conclusions.....72

Discussion..... 72
Field Method Problems..... 72
Unmixing Results..... 73
Conclusions..... 77

References.....79

Appendix A, Numerical Fractions.....84

Chapter 1

Introduction

Vegetation protects the surface of sand dunes in several ways. Vegetation traps particles, provides direct cover, and takes momentum from the flow of air (Bagnold 1954). On the High Plains of the United States, regions of sand sheets and sand dunes have been reactivated at least four times in the past 10,000 years at ca. 9500-5500 yr B.P., 550 to >4800 yr B.P., 4800 to >1000 yr B.P. and, <1000 yr B.P. (Forman, et al 1992; Muhs and Maat, 1993). These dune forms are currently stabilized by vegetation (Lancaster, 1997). Over grazing can deplete the natural vegetative cover as well as alter surface run off which can affect overall rangeland health. Warmer temperatures and dryer conditions, predicted by global climate models, will produce drought-like conditions that cause a decrease in natural vegetation, soil moisture, and evapotranspiration (Forman et al, 1992). Between natural variations in rainfall on the High Plains, potential anthropogenic influences to global climate, large-scale drought in the future is a possibility.

This thesis is part of a larger project that is in progress at the Center for the Study of Earth from Space (CSES). The project undertaken by CSES seeks to assess land and land-use change in a multi-year study of the High Plains in an effort to map areas of potential sand dune reactivation. The study area for that project includes 33 images from each of three different years (1985, 1988 or 1989, and 1996) and an additional fourth year of coverage in some areas with Landsat 7 imagery. In order to study dune reactivation probability, one must be able to quantitatively study the amount of vegetation on dunes. Satellite remote sensing using Landsat 5 and now Landsat 7 imaging systems, provides a means to look at images taken before present and with proper analysis, observe how the vegetation fraction has changed during times of drought and assess the current state of stabilization.

This thesis is a study to ascertain the ability to map sparse vegetation on two High Plains locations using linear spectral mixture analysis on Landsat 7 data with AVIRIS (Airborne Visible and Infrared Imaging Spectrometer) imagery and field data as a basis of comparison. Endmember bundles (Bateson et al, 2000) that include multiple spectra from dominant cover types such as NPV (Non-Photosynthetic Vegetation), green vegetation, and soil, better encompass endmember variability. These bundles are used in a Monte Carlo Unmixing approach that has been developed by Asner and Lobell (2000) and Asner et al (in review). This method, called AutoSMA, uses endmember bundles to derive fractions using linear spectral mixture analysis for each pixel and arrives at a mean cover for each type. A standard deviation, based on the range of fractional cover derived for each pixel, is computed and is the error for the fractions (Asner and Lobell, 2000; Asner et al in review). The

near-simultaneous overflights provide a unique opportunity to temporally constrain the surface conditions and directly compare the spectral mixture analysis results for each sensor. To make the endmember bundles derived with AVIRIS applicable to the Landsat 7 data, the spectra needed to be resampled to the six visible and near infrared bandpasses of Landsat 7 (see figure 2.1 for Landsat 7 bandpasses). These resampled AVIRIS endmember bundles were used to unmix Landsat 7 data are shown to provide the best direct comparison between the two instruments. Mixture analysis with Landsat 7 endmembers yielded reasonable estimates of cover, but with more uncertainty than the use of AVIRIS endmembers. The use of Landsat 7 endmember bundles delivered insight into the limitations and advantages of using Landsat data solely to derive fractional cover for this entire High Plains study area.

The Morgan County dune fields, as well as other major dune formations in Colorado and the High Plains are formed by northwest winds (Stokes and Swinehart, 1997). The Morgan County dunes are parabolic or compound parabolic dunes with arms pointing up wind that can be on the order of several kilometers long, see Figure 1.1, (Forman et al, 1992). Vegetation is usually thickest on the lower slopes and sparse to absent near the nose of the dunes (Pye and Tsoar, 1990). Mapping fractional vegetative cover less than 30% is necessary in predicting dune reactivation since it is beneath 30 % vegetation cover that sand begins saltating (Pye and Tsoar, 1990; Buckley, 1987). The temporal aspect of Landsat Thematic Mapper provides an historical perspective, allowing the study of surface cover under different climatic conditions. One unknown using Landsat TM to study fractional vegetation cover in a

semi-arid region is how accurately it can detect low fractions of vegetation and distinguish NPV (non-photosynthetic vegetation) from soil.

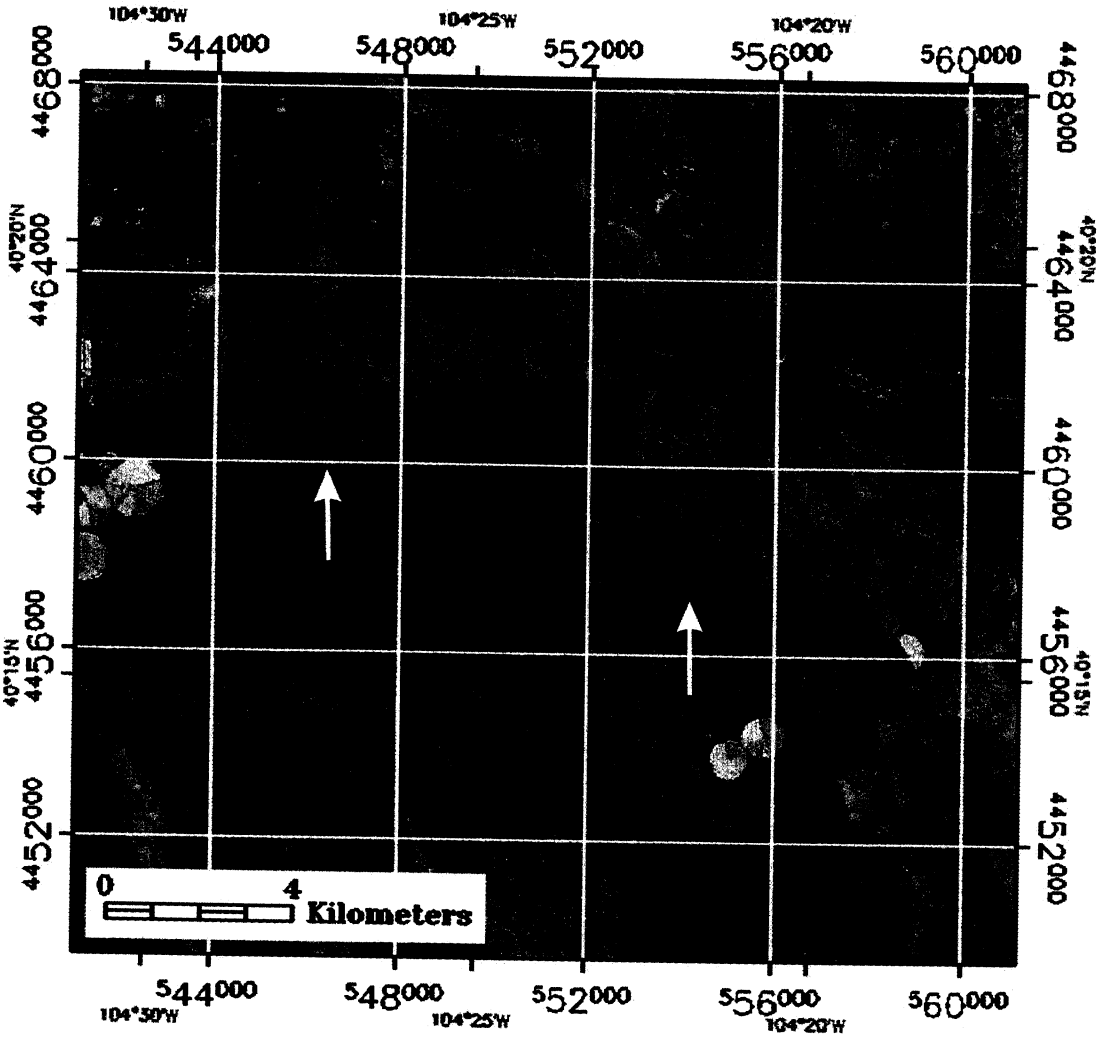

Figure 1.1. A principal component analysis image of the Ft. Morgan Dune Field in the area of the South Platt River. Dark blue, linear-parabolic features are the crests of the dunes.

AVIRIS data were collected on July 10, 1999 near Ft. Morgan, Colorado and on September 30, 1999 near Logan, New Mexico, see figure 1.2. Both of these flights preceded overflights of Landsat 7 on the same days by approximately one hour. The

Ft. Morgan site was selected because it includes regions of linear parabolic, stabilized dune fields, see figure 1.3. The Logan site included regions of active sand dunes with very low vegetation cover, see figure 1.4. A near-simultaneous overflight is important in removing unknowns while comparing the two sensors. Flights that occur on different days introduce atmospheric uncertainty, differences in surface moisture, variations in plant development and senescence as well as canopy structure, and solar elevation and azimuth.

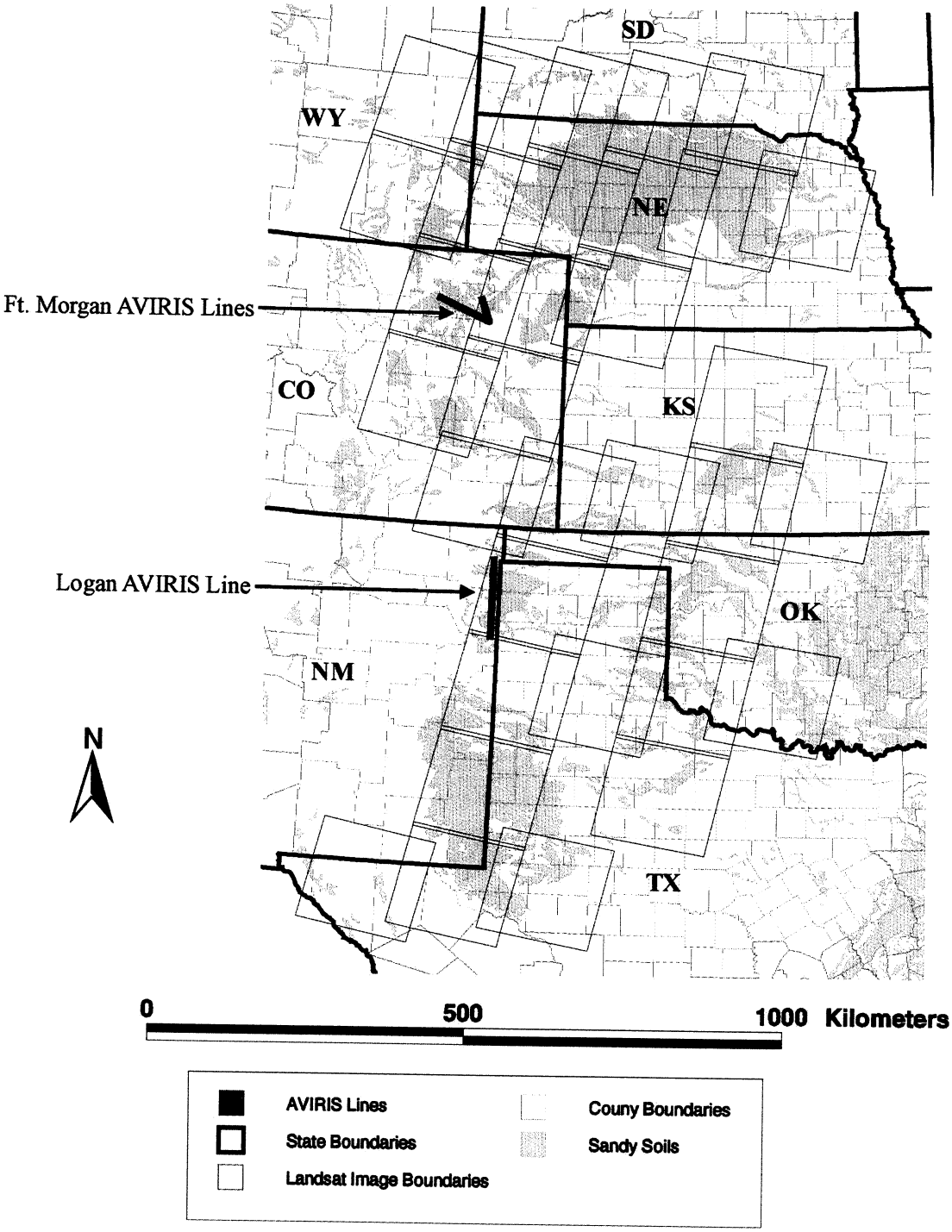

Figure 1.2. Map of the High Plains of the United States.

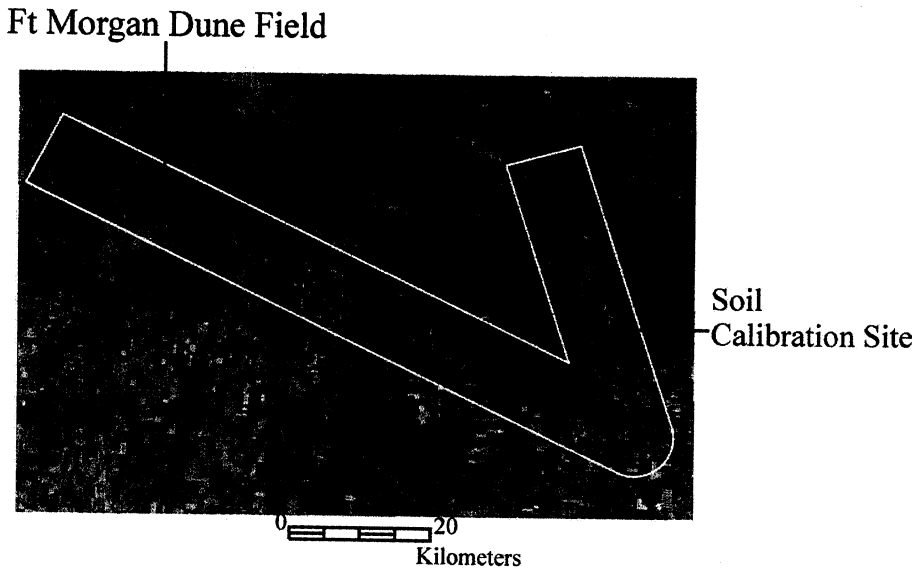

Figure 1.3. Ft. Morgan AVIRIS flight lines overlaid on a Landsat 7 image for July 10, 1999.

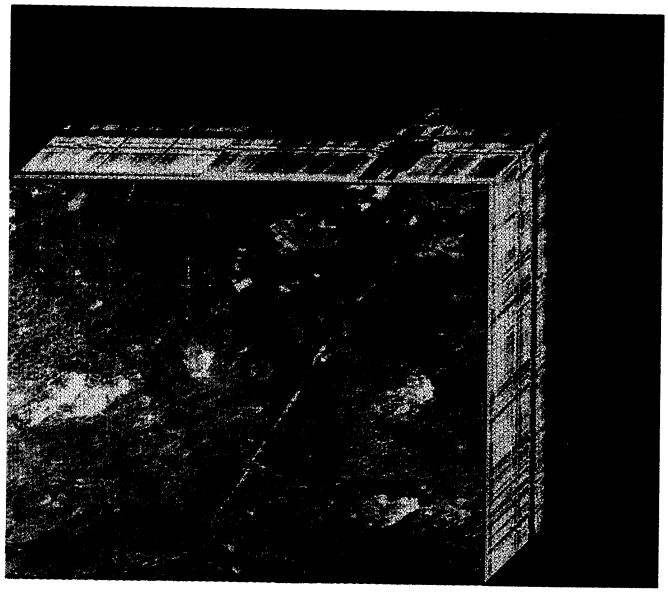

Figure 1.4. AVIRIS 3-d cube of the Logan, New Mexico study site, bright areas are active sand dunes.

Chapter 2

Background

Instrumentation

The Landsat Program has provided continuous mapping of the earth since 1972. The Landsat 5 Thematic Mapper has been in operation since 1984 and is useful in studying change at the human scale in broad areas over time. In April 1999, Landsat 7 was successfully launched and will continue with the long Thematic Mapper history producing multispectral, 16 day repeat cycle images, see figure 2.1 for Landsat 7 bandpasses.

AVIRIS, the Airborne Visible Infrared Imaging Spectrometer, has 224 channels at 10 nm spectral sampling between 370nm and 2510nm and produces a full solar radiance spectrum for each pixel. The field of view (FOV) is 30 degrees, which produces an 11km swath at 20km altitude. The instantaneous field of view is 1 mrad (20m at 20km altitude). AVIRIS covers significantly smaller areas than Landsat, maximally 11km by 800km. The AVIRIS instrument is flown on the ER-2 aircraft platform (for high altitude data), which limits the temporal coverage of the imagery. Data produced by AVIRIS is superior to Landsat in its ability to define unique spectral features with its narrow band sampling, its higher signal-to-noise-ratio, and

the potential to extract greater information content (Vane et al, 1993; Green et al, 1998).

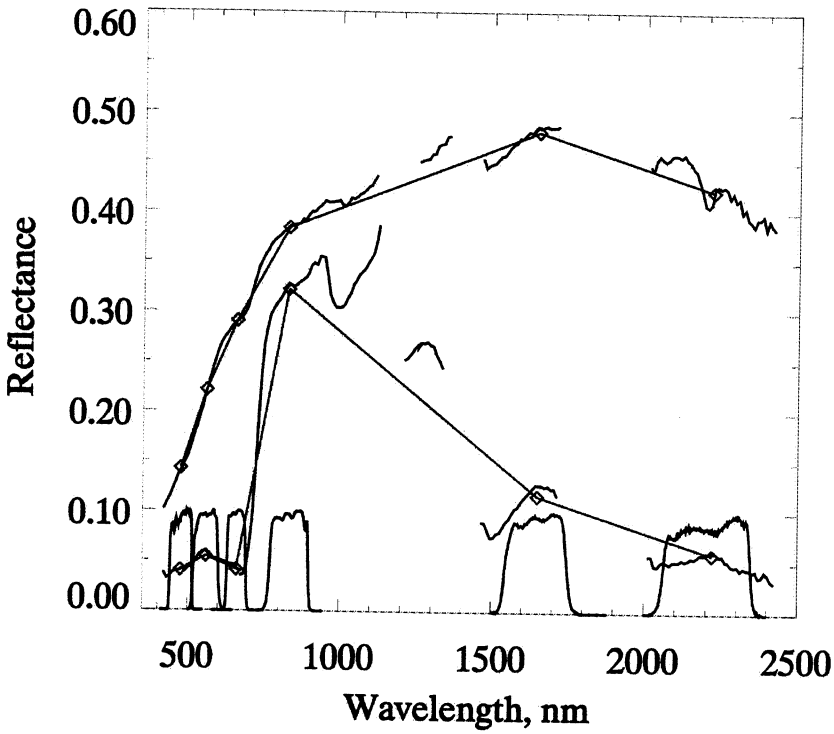

Figure 2.1. AVIRIS spectra, Landsat 7 spectra (red and blue), and scaled Landsat 7 bandpasses.

One of the limiting factors of Landsat TM is the discontinuous spectrum produced for each pixel, see figure 2.1. With continuous spectra, surface materials can be identified more precisely (Goetz et al, 1985). Multispectral imaging systems acquire data across a few broad bands and, as a result, narrow spectral features cannot be resolved or used to accurately identify surface composition.

Spectral Mixture Analysis Theory

Linear spectral mixing assumes that the reflectance spectrum of a pixel is a linear combination of all components in that pixel's GIFOV (Ground Instantaneous Field of View). The spectrally unique features within a pixel, for example, water,

shade, and vegetation are called endmembers (Garcia-Haro et al, 1996). Endmembers may be derived from images or gathered with field or laboratory spectrometers and can be incorporated into a spectral library for use in mixture analysis. There are two fundamental constraints to the theory of linear spectral mixture analysis: (1) The endmember fractions must sum to one and (2) the fractions must be non-negative (Boardman, 1991).

The linear mixture model can be expressed in matrix form as

$$A*x=B \qquad (2\text{-}1)$$

Where

- A = a matrix whose columns contain pure endmembers
- x = a vector of the fraction of each endmember in a particular pixel
- B = the resulting vector that is the linearly mixed reflectance spectrum

(Menke, 1984).

The matrix A is m columns by n rows with the number of endmembers being m and the number of bands being n. The vector x contains m fractions that sum to unity. B, the resulting pixel, has n elements. As long as the number of endmembers is less than the number of bands, the problem is overdetermined and an estimate of the abundance vector x exists (Menke, 1984).

Scale plays an important role on the type of mixing that can occur. On larger scales there is more molecular scattering between materials or transmission through a material and the mixture becomes more non-linear or intimate (Roberts et al, 1993). Areal mixing models assume that within the field of view there is no multiple scattering between materials. Each spectrum is the weighted sum of the reflectance

from each ground component, see figure 2.2 (Settle and Drake, 1993). Few natural systems are entirely linear or entirely non-linear but are a combination thereof (Borel and Gerstl, 1990). The mineral mixtures in rock assemblages can, at the grain size level, be very non-linear, but on a smaller scale the mixture becomes effectively a linear component of the endmembers of resulting pixel. As the scale of the features observed increases so does the linearity of the mixture (Boardman, 1991). While non-linear processes may dominate at one level, the scale of the imagery affects the resulting mixture scheme.

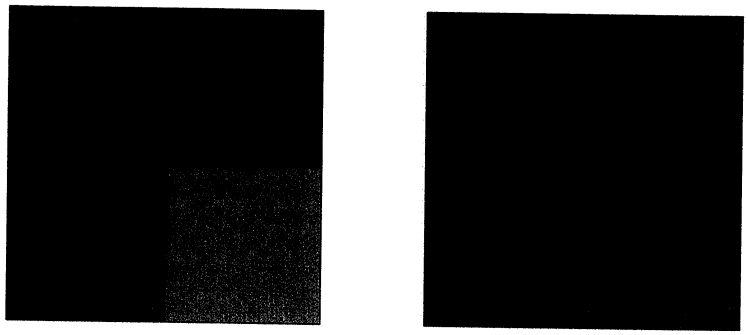

Figure 2.2. Simplistic view of mixed pixel problem.

Spectral Mixture Analysis and Vegetation Mapping

Spectral Mixture Analysis (SMA) has been used with hyperspectral imagery for the purpose of mapping biomass, woody species encroachment, land management practices, fractional cover, distinguishing live from dead plant tissue, and species distribution (Settle and Drake, 1993; Roberts et al, 1993; Wessman et al, 1997; Roberts et al, 1998; Martin et al, 1998; Drake et al, 1999, Lobell et al, in review; Asner and Lobell, 2000). SMA has been performed on multispectral data for the purpose of vegetation analysis under a variety of circumstances (Smith et al, 1990;

Sohn and McCoy, 1997; Adams et al, 1995, Elmore et al, in press, Asner et al, in review). The applications of SMA to multispectral imagery are growing and showing benefits over traditional classification and vegetation indices methods to assess vegetation cover and condition (Elmore et al, in press; Adams et al, 1995).

Moderate range spectral and spatial resolution sensors, such as Landsat Thematic Mapper do not produce data that can be used map areas with sparse vegetation well (Vane and Goetz, 1993, Smith et al 1990). Sohn and McCoy (1997) took field measurements of vegetation fractions in an arid region and compared them to mixture analysis derived from their Landsat 5 data. The Landsat data consistently under-reported vegetation fractions less than 30% (Sohn and McCoy, 1997). The under-reporting of vegetation fraction can be a result of spectral dominance from soil and rocks, as well as the signal-to-noise-ratio of the instrument (Heute, 1985; Smith et al, 1990).

Smith et al (1990) studied the use of SMA in mapping semi-arid vegetation in Owen's Valley, California. The endmembers used in the study were collected in the laboratory and with a portable field spectrometer. These types of reference endmembers have advantages in the pureness of the spectra that can be collected. One flaw with using reference endmembers is the uncertainty of representation of actually plant canopy reflectance, which has significant contributions from plant structure (Asner, 1998). Smith et al (1990) showed a reasonable correlation with field-measured green vegetation and image derived fraction of vegetation with r^2 values ranging from 0.64 to 0.85 for the six images used. Though the fractions do correlate, the image estimates of live vegetation cover always overestimated these

abundances. Despite these differences, Smith et al (1990) concluded that SMA is useful in studying changes in green vegetation abundance, as the results were spatially consistent with the projected amount of vegetation cover.

Elmore et al (in press) undertook a study to determine the precision and accuracy of using SMA to study vegetation change in a semi-arid environment. They used four invariant endmembers, two green vegetation spectra and two soil spectra, for unmixing six Landsat 5 images from six years. By keeping the endmembers constant, they were able to determine absolute change from these baseline endmembers. Their study showed good agreement (r^2 of 0.88) of field collected percentage live cover and Landsat 5 image derived percentage live cover, uncertainty of ±4.0% of the live cover measured in the field.

In addition to studying the precision of SMA to study green vegetation changes, Elmore et al (in press) also compared NDVI (Normalized Difference Vegetation Index) calculations of change. While NDVI values do correlate well for a single date (r^2 of .83 with field measurements), the relationship of NDVI to the field measurements was less robust than SMA when measuring changes between scenes. This effect can be attributed to soil brightness effects on NDVI, which can be as much as 0.3 with changes in bare soil NIR reflectance (Heute et al, 1985). Wessman et al (1997) explained that canopy geometry, background materials, non-photosynthetic vegetation, and percentage cover can all affect the response of NDVI. While a good indicator of greenness, NDVI results do not discriminate the different types of landscape cover or fractions as well as mixture analysis can.

One problem with using SMA with multispectral imagery is distinguishing NPV (which includes bark, dry leaf material, wood, and stems) from soil. The spectra can be very similar and in many cases the "pure" soil or "pure" NPV endmember may have contributions from one cover type or the other. Green vegetation is easily distinguished from both soil and NPV, but often NPV spectra will be mixed with green vegetation spectra simply by being underneath the green tissue of plants (i.e. stems). Of the following studies of unmixing Landsat TM data only Adams et al (1995) and Asner et al (in review) included an NPV endmember: Smith et al, 1990; Sohn and McCoy, 1997; Adams et al, 1995; Elmore et al, in press; Asner et al, in review. In this study, quantifying the NPV fraction in relation to the fraction of soil is necessary in determining how much bare soil is unprotected.

Dune Stabilization

Vegetation on dunes creates a surface roughness that causes drag on wind and more surfaces on which sand grains can accumulate. This surface roughness substantially reduces the ability of the wind to erode the sand (Bagnold, 1954). Sand transport is a function of the supply of sand, wind velocity, and natural vegetation cover. No substantial sand movement takes place when vegetation fraction cover is higher than approximately thirty percent (Pye and Tsoar, 1990; Buckley, 1987). Buckley (1987) used the results of wind tunnel experiments to determine the threshold velocity of sand movement with the influence of vegetation:

$$U_{vt}=Ut/(1-kC) \qquad (2\text{-}2)$$

Where

- Uvt = the threshold velocity on sand with vegetative cover C.
- Ut = the threshold velocity of bare loose sand (~3.3 m/s).
- K = constant dependent on plant shape (for small herbaceous plants, K=0.018, for small, round, stemless plant, K= 0.046)
- C = the percentage vegetation cover (up to 17%)

(Pye and Tsoar 1990; Buckley 1987).

For a landscape dominated by herbaceous species (k=0.018) and a fractional cover of 15% the threshold velocity would be 4.52 m/s (approximately a 10 mph wind). Wind velocities on the High Plains exceed threshold sand movement velocities 30-60 % of the time (Gillette and Hanson, 1989).

Spatial Characteristics

Another consideration in the calibration and use of remotely sensed data is the PSF (Point Spread Function) of the sensor. The sensor total PSF is a weighting function that approximates the signal that comes from out side the sensor's GIFOV. Blurring occurs from the combination of the sensor's total PSF, optics, electronics, and detectors. Geometric distortions also affect the PSF. As a result of the PSF, the GIFOV of Landsat TM instruments is effectively 40-45 meters, indicating that 25 to 30 % of the signal in a given pixel came from outside of the $900m^2$ surface area the pixel is representing (Schowengerdt, 1997).

The spatial response uncertainty is 10% of the IFOV of AVIRIS. This means that nominal pixel size of 1 mrad of AVIRIS is accurate to 0.1mrad (Green et al, 1998). This is not the PSF of AVIRIS, but the spatial accuracy of the pixel. An AVIRIS pixel's IFOV is a gaussian function, with 1 mrad being the full width half

maximum of the gaussian. The PSF can be approximated from the gaussian with as much as 33% of the signal coming from outside the geographic area of the pixel, yielding a ~1.3 mrad IFOV and a 26m by 26m pixel size at 20km altitude (Chrien et al, 1991; Schowengerdt, 1997). Both the spatial uncertainty and the PSF need to be recognized while performing pixel based processing and any attempt to quantify singular points of an image. Calibration targets need to be large and homogenous to account for the sensor PSF and not have spectra "contaminated" by neighboring substances.

BRDF

BRDF, the Bidirectional Reflectance Distribution Function, is the reflectance at multiple view angles at a given time and solar position (Walthall et al, 1985). Physically, BRDF is the directional radiance reflected from an object, divided by the irradiance at a specific incident angle (Diner et al, 1999). BRDF is determined by several factors including solar geometry, scanner geometry, flight line/image orientation, and surface composition. Surface components, soil, green vegetation, NPV, and water all have different inherent BRDF properties. Plant canopy BRDF is a function of tissue structure, foliar orientation, stem and leaf angle distribution, and species spacing and distribution (Asner et al, 1998; Li and Strahler 1985). Soil BRDF properties are a function of particle size, particle distribution, mineral components, surface roughness, and relief (Jacquemond et al, 1992). In order to characterize the unique BRDF qualities of surface materials, measurements of BRDF can be made with a goniometer, which measures reflectance at different zenith and azimuthal angles (Deering, 1989).

Flight line orientation relative to the sun can have a large effect on the radiance that is recorded at the sensor (see figure 2.3 for schematic AVIRIS scan). If flight lines align with the azimuth of the sun, the scanner is never looking in the direction of the sun; the sun is effectively behind or directly in front of the aircraft. If the flight lines are oriented more perpendicular with respect to the principal solar plane, the sensor scans toward the sun and away for the sun. When the flight lines are perpendicular to the solar plane there is a relatively higher reflectance on one side of the scan. A bias of this type is also dependent on the individual surface materials, boundaries, illumination, and orientation which determine whether the incoming light is scattered back toward the sun or scattered forward (away) from the sun (Kennedy et al, 1997; Goetz et al, in press).

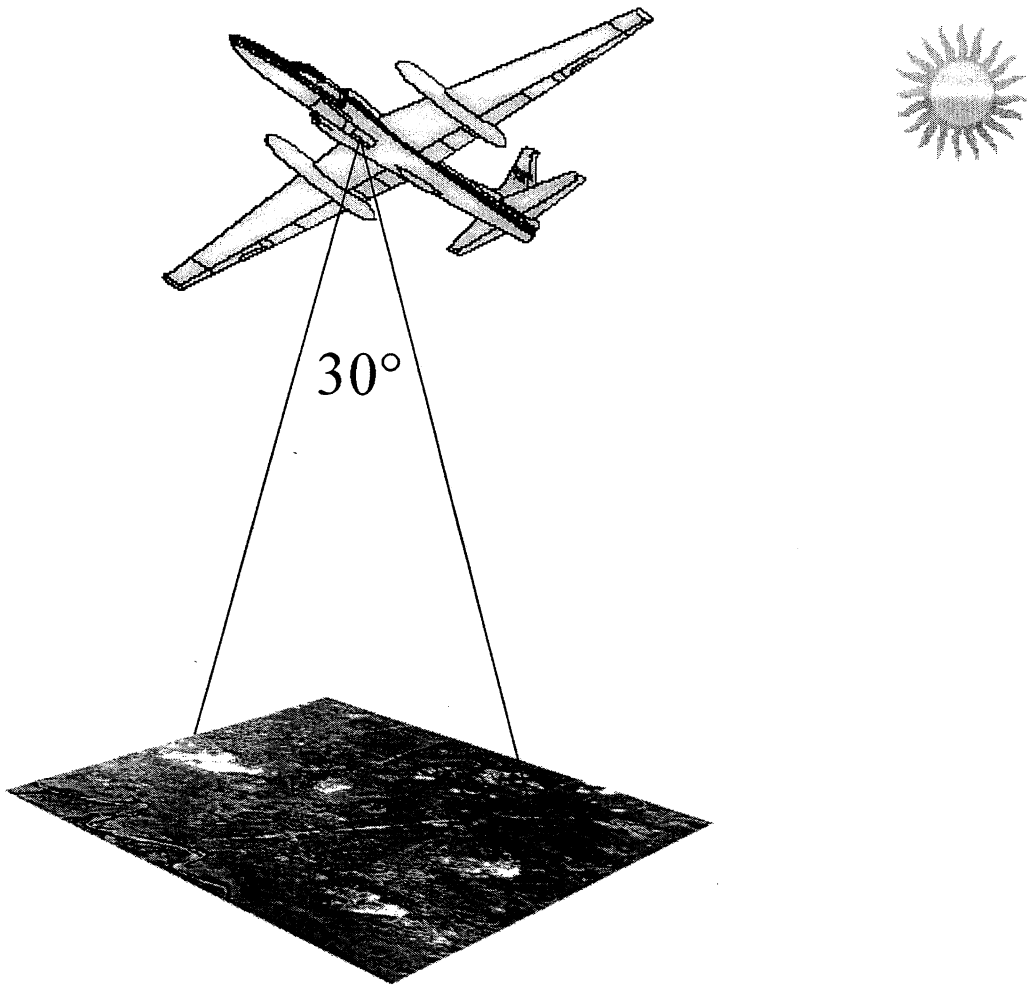

Figure 2.3. Schematic of an AVIRIS scene, the spectra at the edges of the scan (furthest from nadir) can deviate from the spectra of the same cover type that are imaged at nadir due to the orientation of the flight line with respect to the principal plane of the sun.

Atmospheric BRDF effects are associated with column water vapor scattering and absorption as well as aerosol scattering. Sensor view angle and scan angle relative to the sun can increase the atmospheric path length and scattering interactions. Goetz et al (in press) shows that atmospheric scattering associated with scan angles can have an effect on the reflectance of shorter wavelengths (<500nm), but this effect is far less than the total observed BRDF. Atmospheric correction

algorithms, such as dark object subtraction and ATREM correct for path radiance, but do not directly account for atmospheric BRDF.

Physical and Climate Settings

The climate of the area surrounding Logan, New Mexico is classified as semi-arid and continental with seasonal changes and widely varying diurnal temperatures. This area typically has very low humidity and clear skies and receives approximately 380 mm of precipitation per year. The study site in the Logan AVIRIS line is dominated by the presence of dune sand and very sparse vegetation on the dunes. Regions of Tivoli fine sand and Brownfield fine sand surround these dunes, which are Entisols (soils without pedogenic horizons) and Alfisols (gray or brown surface soils with subsurface clay), respectively (Birkeland, 1984). The natural vegetation growing in this region include tall grasses, *Artemisia filifolia* (sand sage), *Yucca Baccata* (yucca), *Rhus trilobata* (skunkbush sumac), *Andropogon hallii* (little blue stem), *Andropogon gerardii* (big bluestem), and *Prosopis L.* (mesquite) (USDA, 1974). In the surrounding area there is dry land farming, irrigated framing, and cattle ranching—approximately 8000 head graze the region used in this study.

The Ft. Morgan area is a semi-arid continental region with low humidity and a relatively low mean annual rainfall of 330 mm. In this region approximately 80% of the precipitation falls between April and September. The dunes in this region are part of the Valentine Sand series that is characterized as loamy sand and sand and are part of the Entisol order. The natural vegetation that grows on these dunes is dominated by short grasses, *Helianthus annuus* (sunflowers), *Artemisia filifolia* (sand sage), *Yucca Baccata* (yucca), *Andropogon hallii* (sand bluestem) and *Calamovilfa*

longifolia (sandreed) (USDA, 1968). This soil can support some crops but proper soil and water conservation practices are needed for favorable yields.

Chapter 3

Methods

The method for comparing the ability of Landsat 7 to map vegetation relative to fractions derived with fieldwork and AVIRIS imagery is as follows:

- Field site selection
- Field measurements on or near the time of the overflights
- Processing of field data
- Request and receipt of imagery
- Atmospheric correction
- Data specific processing
- Comparison of results

Vegetation Measurements

The vegetation site used with the Ft. Morgan imagery was selected using a September 17, 1998 Landsat 5 image. Areas with relatively sparse vegetation were identified as well as areas containing parabolic dune forms (See Figure 1.1). The property visited belongs to the Lost Creek Cattle Company of Roggen, Colorado. This company operates a cattle ranch on the land and has implemented a rotational

grazing system to reduce the soil erosion. The site used with the Ft. Morgan data had not been grazed since the previous summer. As another point of comparison, a region of active sand dunes was selected north of Logan, NM. From visual estimates, the most vegetation on these dunes is 15 % cover. Cattle also graze this region.

A 100m x 100m area was determined to be the minimal size for the vegetation plot in order to encompass over 9 of the 30m by 30m Landsat 7 pixels and thus account for the PSF of the instrument. The 100m by 100m plot was chosen arbitrarily at the Ft. Morgan site. The vegetation site was known to be located within the AVIRIS flight lines and was in a stabilized dune region, see figure 3.1. The Logan 100m by 100m plot was specifically chosen as an active dune for the purpose of measuring sparse vegetation.

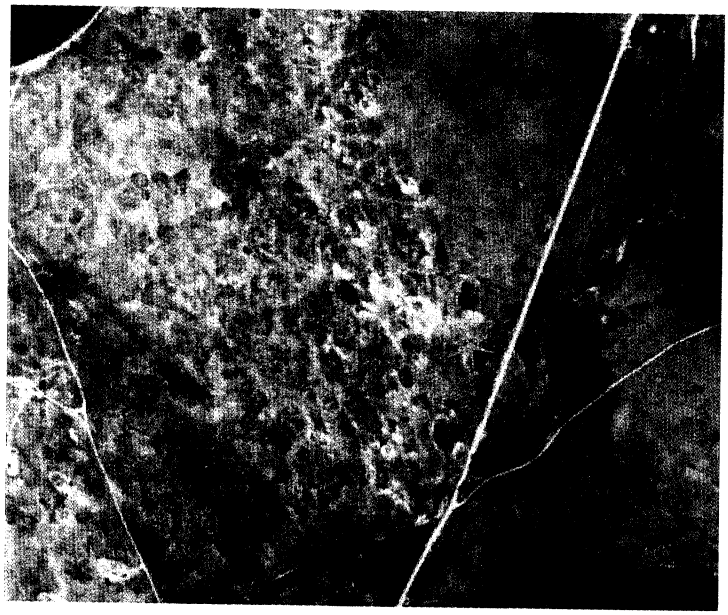

Figure 3.1. Roggen vegetation study site marked with yellow star.

The site was established by staking the corners using a measuring tape. Every ten meters along the perimeter a flag was placed. At each corner GPS measurements

were made to locate the plot in geocorrected images. Over one hundred GPS measures were made at each corner in order to have a more accurate point upon differential correction.

A line intercept method was selected as the best way to measure the vegetation of stabilized sand dunes. Other methods, such as the point intercept and boom photography were considered but were deemed susceptible to larger error because of the methodology. The point intercept method uses a dropped pin and the first substance the pin encounters is recorded (Phillips, 1959). This method can give a misinterpretation of the percent cover in sparsely vegetated areas since the placement of the frame determines what cover type is recorded. The boom photographic concept utilizes a camera on a pole to photograph the ground cover. Image processing is used on the photos to determine the ground cover fraction. The photographic method complicates the primary analysis with secondary analysis.

The line intercept method uses a measuring tape laid out flat. In 10 m increments, along the 100m transect, an observer records the physical length of vegetation, NPV, and soil, see figure 3.2 (Phillips, 1959; Smith et al, 1990). The 100 m transects are made 10m apart. This method, while giving total cover, also forms a grid of information over the plot.

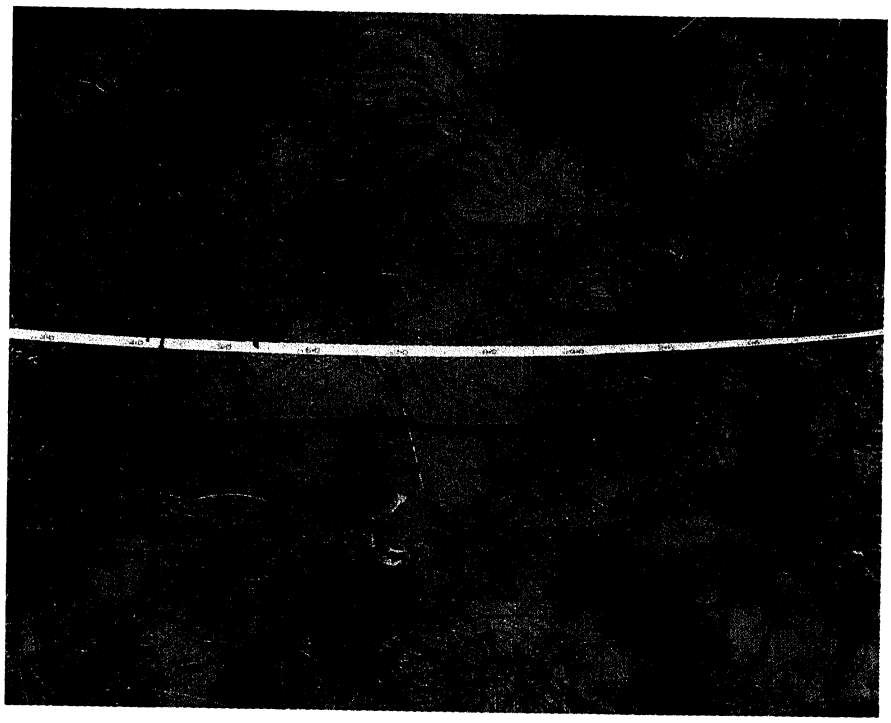

Figure 3.2. Measuring tape at Ft. Morgan vegetation study site.

Spectral Characterization Procedure

In addition to determining fractional cover of the Ft. Morgan vegetation site, the plot was measured with an Analytical Spectral Device (ASD) Fieldspec-FR™ instrument to spectrally characterize the vegetation. The ASD samples the solar reflected spectrum ranging from 350 to 2500 nm, with 1nm sampling and 2151 continuous channels. The reflectance data gathered with the ASD were used to compare the retrieved reflectance of the AVIRIS and Landsat 7 data to field collected surface reflectance, see figure 3.3.

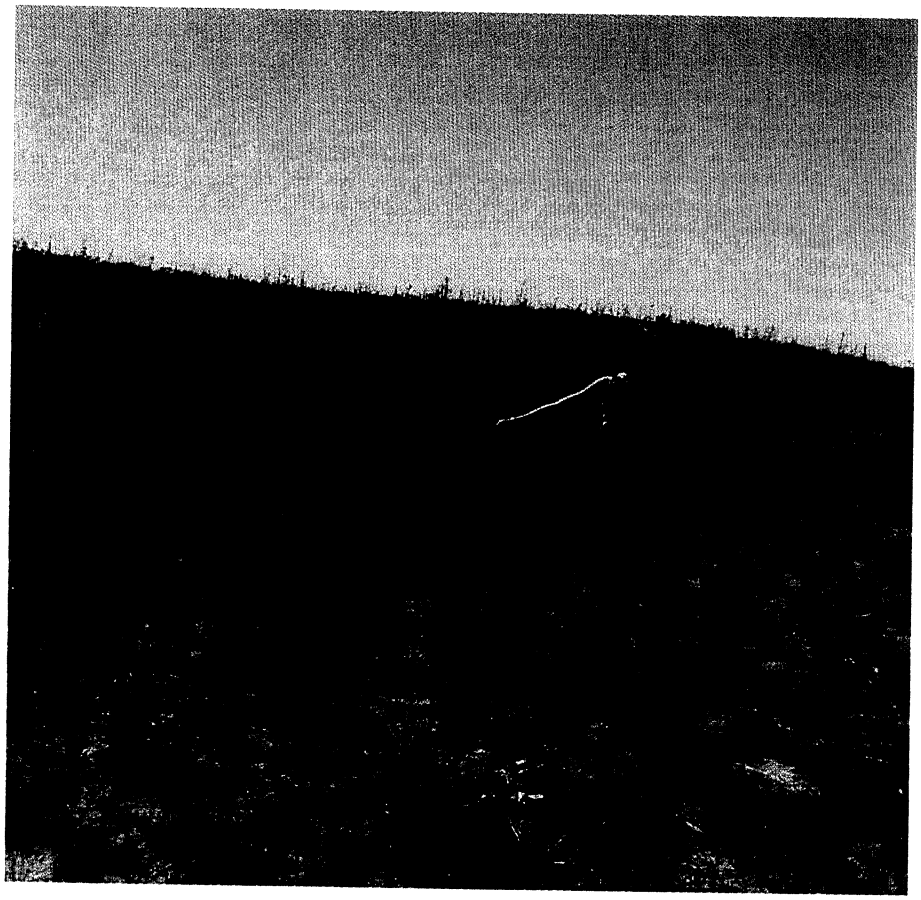

Figure 3.3. Vegetation spectral characterization with a portable field spectrometer.

Spectra were collected using the following method. The Field Spec-FR™ was "warmed up" while travelling to the site (approximately one-hour). Once arriving at the site the instrument was configured to average 50 spectra per measurement, 50 measurements per dark current measurement and 50 measurements per white referencing. An 18-degree foreoptic was chosen since the ground footprint is approximately 30cm and is more suited for measuring a large region. A five inch Spectralon® panel was used a reference standard. East-west transects were chosen since there is less scattering off the user from the sun into the field of view of the foreoptic. A 100m line was traversed; the instrument was calibrated to the Spectralon

standard following each run. The user then moved north 10m to begin the next line, switching the hand holding the foreoptic so as not to shade the field of view of the foreoptic (Curtiss, Personal Communication 1999).

Atmospheric Correction and Calibration

The signal that is detected by the airborne or spaceborne sensor is radiance. Solar radiation passes through the atmosphere twice before being received at the detector, once on the way from the sun to the surface and then reflected from the surface back to the sensor. The radiance that is recorded at the detector needs to be calibrated to surface reflectance in order to remove the atmospheric components that dominate the radiance spectrum. For hyperspectral imaging systems, methods such as ATREM (the ATmospheric REMoval Program) (Gao et al, 1993), use atmospheric absorption features present in the data themselves as well as exo-atmospheric solar irradiance to correct radiance to reflectance data. Once this process is complete, other methods, such as a ground calibration or spectral smoothing methods such as EFFORT (Empirical Flat Field Optimal Reflectance Transformation) are used to remove systematic and modeling errors introduced by ATREM (Goetz et al, 1997).

Landsat data are acquired in digital number (DN). To atmospherically correct Landsat data where there is no available surface reflectance, the DN can be inverted, using spacecraft data (if available), to units of radiance. Once these data are in radiance then the atmospheric effects can be modeled and radiance converted to reflectance.

Atmospheric correction of remotely sensed data does not always require in situ measurements. The atmospheric scattering needs to be removed from the

wavelengths affected by scattering and the radiance data or DN need to be related spectrally to well characterized surface materials. The Dark Object Subtraction (DOS) theory of removing atmospheric scattering postulates that some pixels are composed entirely of shade and the signal recorded at the sensor is due to path radiance (scattering) rather than the actual object on the ground (Chavez, 1996). By subtracting the value of the darkest pixel in an image from the bands that experience the most scattering (i.e. Landsat Bands 1-4), path radiance can removed from an image without contemporaneous ground measurements. DOS is a simple, yet robust, and widely used method of performing in-scene atmospheric correction.

Surface reflectance measurements can be used in an empirical line method (see equation 3-2) to remove the modeling and systematic errors from the ATREM-derived reflectance spectrum as well as calibrate dark-object-subtracted DN to reflectance (Conel, 1987; Clark et al 1993).

$$m=(y/x)-b \qquad (3\text{-}2)$$

Where

- m = Slope
- x = Surface reflectance (in situ) of calibration target, measured with a field spectrometer
- y = DN of calibration target
- b = Offset (following DOS or other path radiance corrections, this term would be zero)

With the offset being zero, the ratio of the DN to the surface reflectance becomes a correction factor to be applied to the entire image to retrieve surface reflectance.

Surface reflectance measurements to calibrate the Ft. Morgan scenes were collected at 11:30 a.m. at Pawnee Power Plant in Brush, Colorado and at 12:30 p.m. at David Wagers' farm in Brush, Colorado, see figures 3.4 and 3.5. Surface reflectance measurements were made at a white ash field and a brown ash field at the power plant, but post processing indicated these regions were not homogenous targets. Ground calibration target measurements at Logan, NM were made 14 days after the overflight on a sand dune, see figures 3.6 and 3.7. ATREM was performed on the Ft. Morgan and Logan AVIRIS scenes, followed by a ground calibration (using the slope correction from equation 3-2). The Landsat 7 data was dark object subtracted and then was calibrated to surface reflectance with the slope correction from equation 3-2.

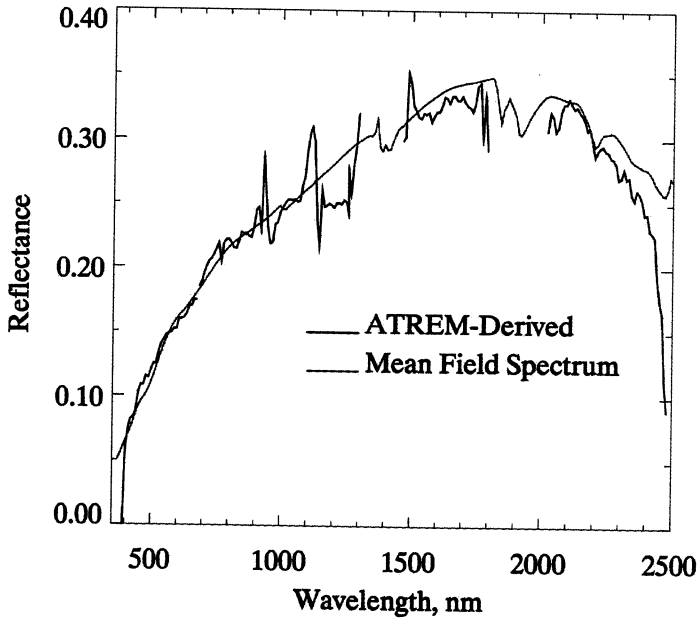

Figure 3.4. Surface and derived reflectance for a bare soil field. in the Ft. Morgan AVIRIS Lines

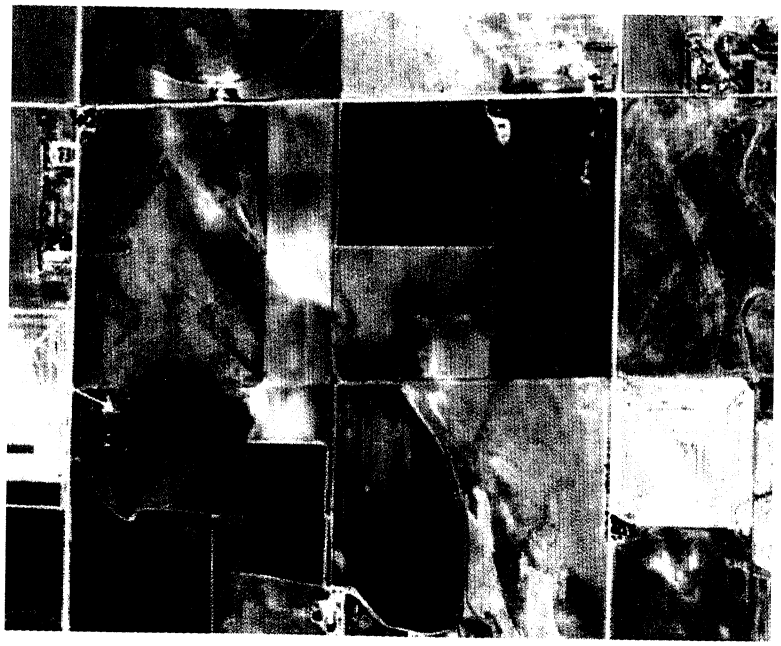

Figure 3.5. Yellow star marks the part of the field where surface reflectance measurements were taken with a portable field spectrometer.

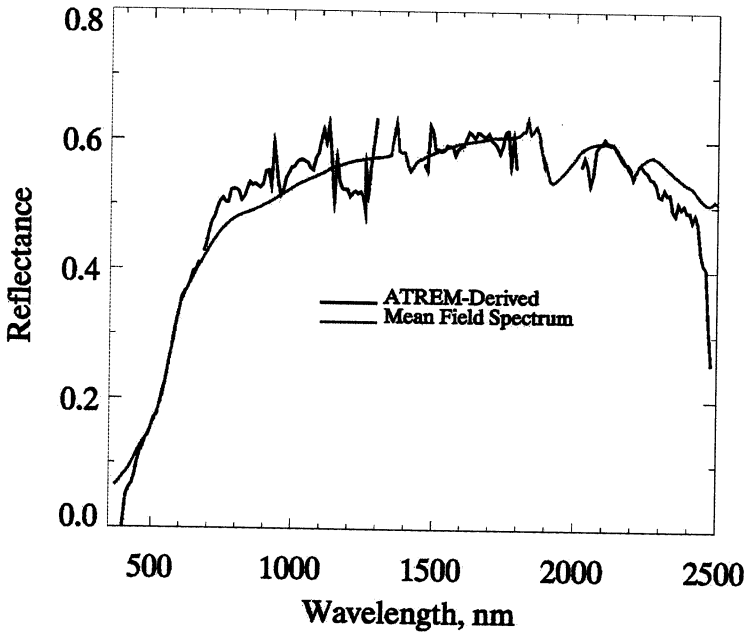

Figure 3.6. Surface and derived reflectance for a sand dune north of Logan, NM

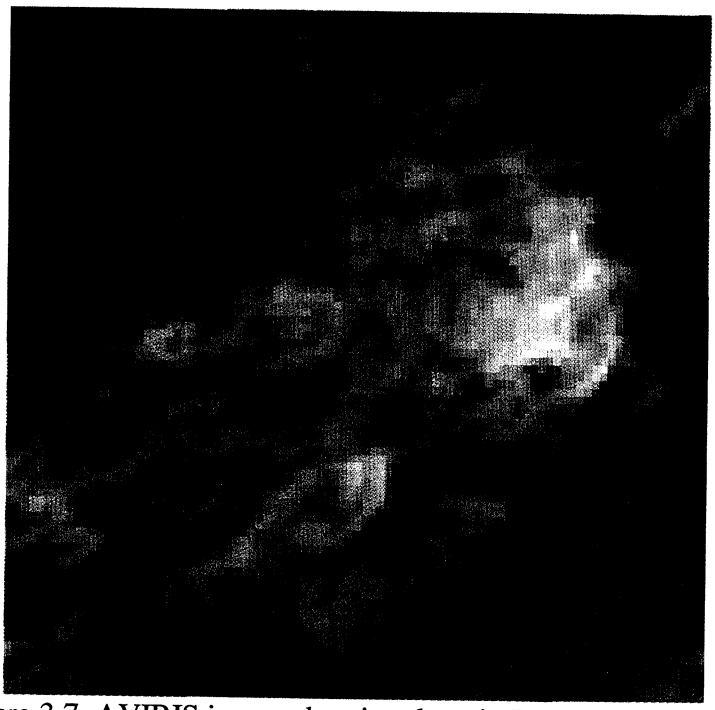

Figure 3.7, AVIRIS image showing dune in Logan scene where calibration measurements were made.

Geometric Correction

In order to make the AVIRIS scenes used in this study comparable to the Landsat 7 images, the AVIRIS data had to be geocorrected. Even though these data were acquired on the ER-2, a stable, high altitude aircraft, there was significant pitching in the imagery. In 1999 the ER-2 used to collect AVIRIS imagery had a GPS-INS mounted on-board. With the data collected from the GPS-INS, precise location of each pixel can be achieved. The Boardman Algorithm for geocorrection utilizes these data to "move" pixels to the proper spatial location (Boardman, 1999). The Landsat 7 data were resampled using the nearest-neighbor technique to match the 17.2m and 15.6m pixels of the Ft. Morgan and Logan AVIRIS pixels, respectively. Resampling to the dimensions of Landsat 7 to AVIRIS using nearest-neighbor was performed to preserve the integrity of the AVIRIS data since these data are the basis

of comparison in this study. The AVIRIS data, once positionally corrected using the Boardman algorithm, were warped using hand picked ground control points to Landsat 7 geocorrected imagery for better agreement using nearest neighbor resampling to best preserve the radiometry of the AVIRIS data.

To ensure that geometric correction was properly performed and to look at the differences in the sensors, the AVIRIS data were convolved to Landsat 7 bandpasses and plotted against each other for each scene used in this study. All scenes are well correlated and clustered indicating minimal geometric variations between the two sensors. Points outside the data cloud are due to misregistration of linear features. Bands 3, 5 and 7 for all scenes were more offset than the others toward higher Landsat 7 values for the same pixel than AVIRIS, see figure 3.8. All the Ft. Morgan scenes were calibrated to the same surface reflectance measurement taken 2 hours after the AVIRIS flight and one hour after the Landsat 7 overpass. AVIRIS reflectance values should theoretically be higher since they were "boosted" more relative to the Landsat 7 data which were acquired closer in time to the soil calibration measurement. The images were ratioed to locate differences between the two scenes, see figure 3.9. Different cover concentrations can be separated in the ratio images, indicating that the BRDF is the probable cause of the offset in the scatter plots. If the ratios were brighter on one side of the image or the other, then scan angle with relation to the sun would be the problem. This is not the case and it appears that the different landforms and cover types are reacting differently to the different sun angles at the time each image was recorded.

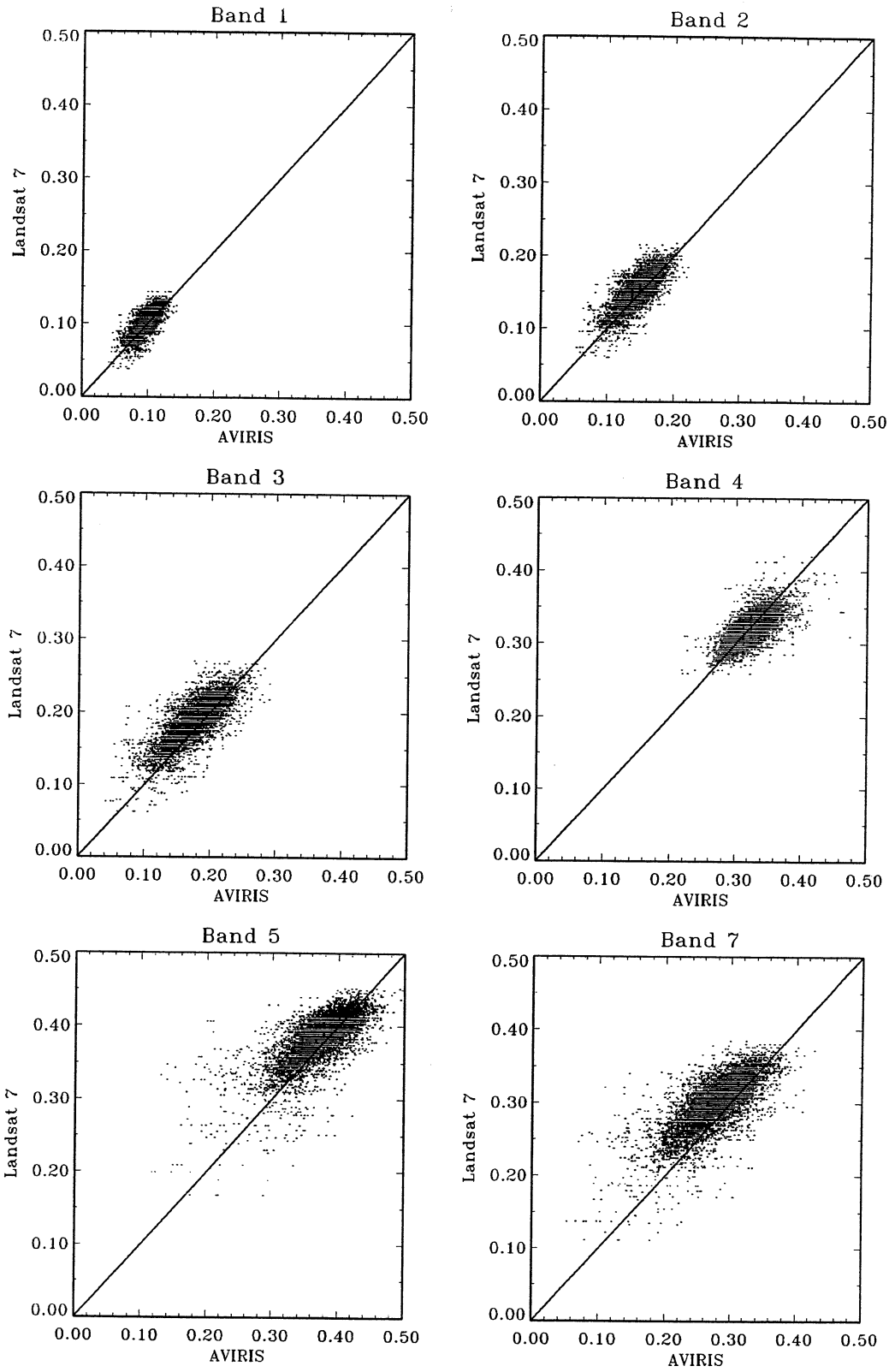

Figure 3.8. Scatter plots of Landsat 7 bands versus AVIRIS convolved to Landsat 7 bands for run 2 scene 10 of the Ft. Morgan AVIRIS lines.

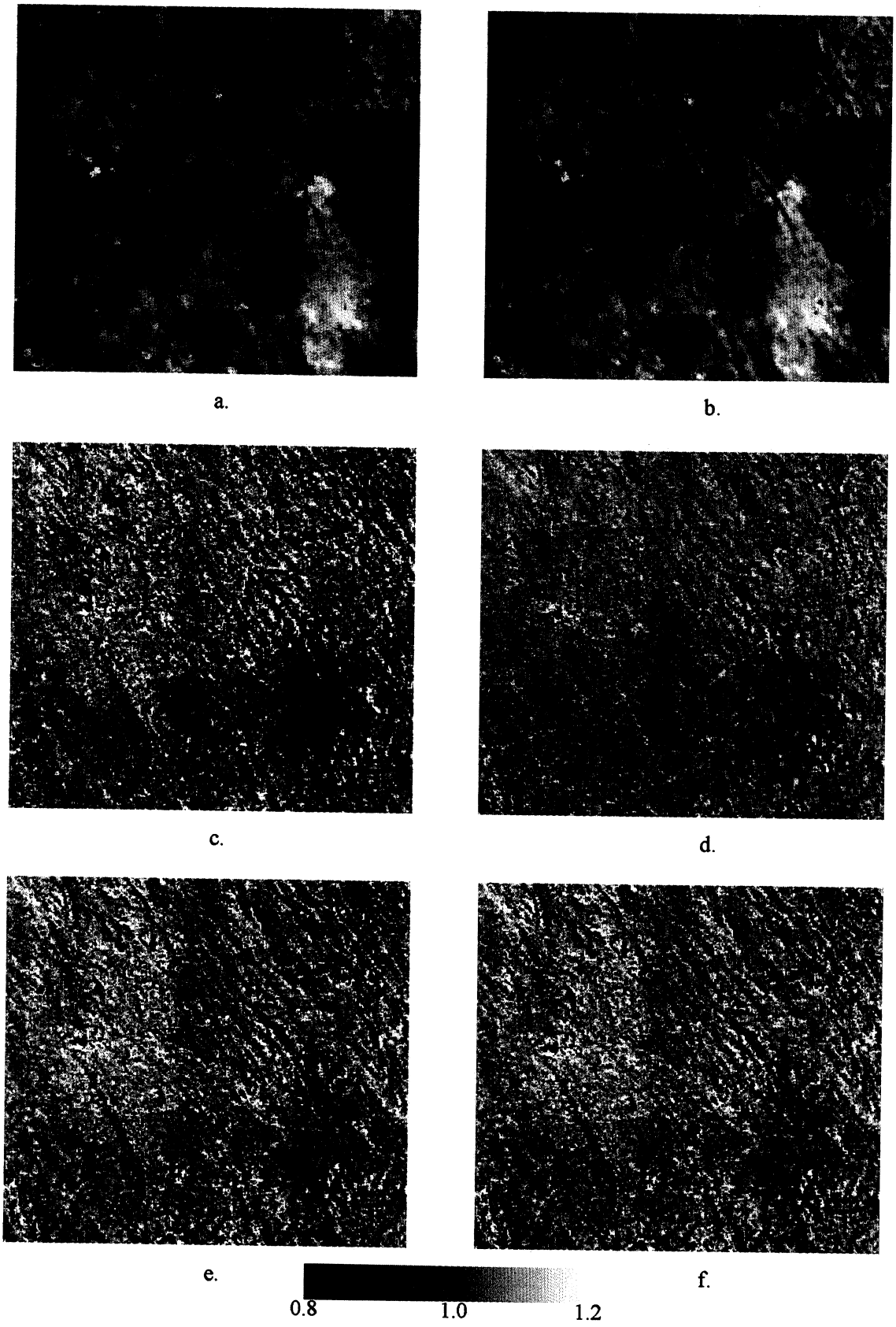
a.
b.
c.
d.
e.
f.
0.8
1.0
1.2

Figure 3.9.

a. Landsat 7 CIR (Color Infrared) image of run 2 scene 10, b. AVIRIS (convolved to Landsat 7 bandpasses) CIR image, c. Ratio of TM band 3 over AVIRIS, d. Ratio of TM band 4 over AVIRIS, e. Ratio of TM band 5 over AVIRIS, f. Ratio of TM band 7 over AVIRIS. A gaussian stretch was applied to the color infrared images. A two-percent stretch was applied to all the ratios to enhance contrast. The linear features in the CIR images are the wings of the parabolic dunes; the brighter areas on these dunes indicate, in the CIR image, that there is less green vegetation. These regions are darker in the ratio images indicating that the AVIRIS values are higher than the Landsat 7. The large bright area in the lower right of the CIR images is easily identifiable in all the ratio images; this region is one of high percentage of NPV (according to mixture analysis and looking at the spectral shapes). Concentrations of vegetation and soil can be detected in the ratio images with careful inspection. The separability of different cover types in the ratio images is a good indicator that the BRDF of the individual cover types' is one of the causes of the offsets in the scatter plots.

Endmember Selection

Selection of the endmembers was assisted with the use of ENVI®, an off the shelf image processing package. A Minimum Noise Fraction (MNF) transformation was first performed on the scene (Green et al, 1988; Boardman and Kruse, 1994). An MNF transform is essentially two principal component transforms where the first transform decorrelates and rescales the noise in the data; this results in the noise having unit variance and no band to band correlation. The second transform is a principal component analysis of the noise-whitened data. The dimensionality of the image can be approximated by looking for large eigenvalues (greater than one) and coherent eigenimages, bands meeting these constraints should be considered dimensionality significant.

To find the purest pixels, the bands with coherent eigenimages were processed with a procedure called the Pixel Purity Index (PPI). PPI involves taking the MNF

transform result and projecting the data onto random unit vectors, the extreme pixels for each projection are "marked" and the number of times each pixel is found to be extreme is noted. The purer pixels are found to be extreme more often than mixed pixels are the result is based on principles of convex geometry where the values of a pixel for a given band have a coordinate in N-d space. The edges and corners of the data cloud in n-d space define the boundaries of a mixing simplex where all the points inside the simplex are a linear combination of the pure endmembers, see figure 3.10, (Boardman, 1993: Boardman et al, 1995). The purest pixels were input into ENVI N-Dimensional visualization and endmembers were selected from the corners of the simplex. "Endmembers" that were obvious mixtures were not used in this study, i.e. spectra that clearly have a green vegetation signature yet in the SWIR2 (2100-2400 nm) region have a clay absorption feature. Non-linearities in the data do not follow linear mixture models and hence produce anomalous "pure spectra".

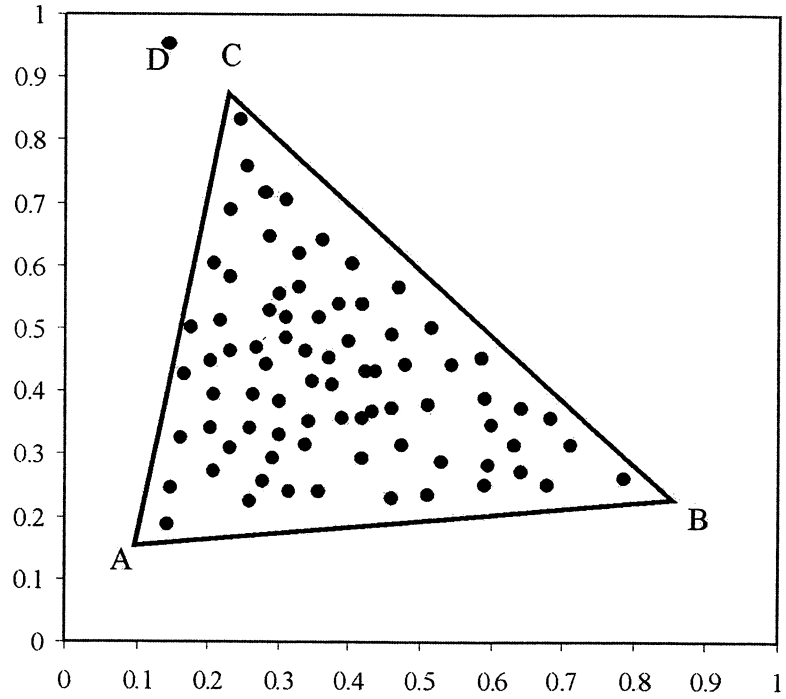

Figure 3.10. Convex geometry example. The points interior to the triangle are unit sum, linear combinations of the endmembers, A, B, and C. Point D is beyond the mixing surface. The resulting fraction of point D would be a greater than one fraction of endmember C. A triangle is the best fitting simplex for these data contained inside of it. Adapted from Boardman, 1993.

AVIRIS endmembers were sorted into three bundles during the selection process. These bundles are green vegetation, NPV, and soil. The concept of bundling endmembers, developed by Bateson et al (1998 and 2000) is a means for accounting for the inherent variability in single pixels. The variability that is contained in vegetation canopies makes it nearly impossible to unmix for a single green vegetation endmember. There is multiple scattering involved, different reflective properties of different tissues, structural canopy attributes, and other properties that contribute to the resulting vegetative spectrum of the pixel (Asner, 1998). By incorporating bundles that represent the dominant cover types of given region (for this study, green

vegetation, soil, and non-photosynthetic vegetation) the variability that is contained within each pixel is taken into consideration more thoroughly (Bateson et al, 2000).

Each bundle included the purest spectra for that cover type as identified with PPI. Image endmembers can never be pure in a semi-arid eco-system, so the purest pixels are effectively mixtures. A shade endmember was not selected as a bundle because with image endmembers, shade is included in the "pure" pixel spectrum (see figure 3.11). Once AVIRIS endmember bundles were compiled, they were convolved to Landsat 7 bandpasses (see figures 3.12, 3.13, and 3.14 for endmember bundle examples) for use in unmixing the Landsat 7 data. Landsat 7 endmembers for each scene were selected using the same methods for determining the dimensionality, purest pixels, and using visualization to find endmember bundles. The AVIRIS endmembers that had been convolved to Landsat 7 bandpasses served as a reference to appropriately separate NPV and soil endmembers, which can be confused with Landsat spectra.

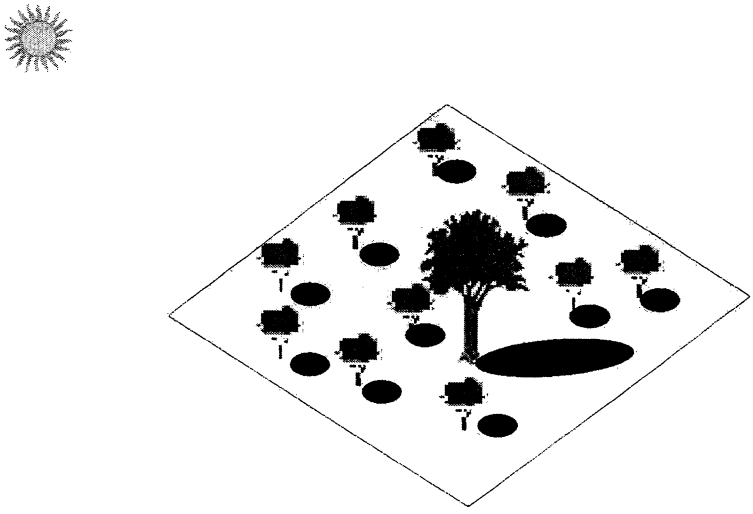

Figure 3.11. A "green vegetation" pixel with shade.

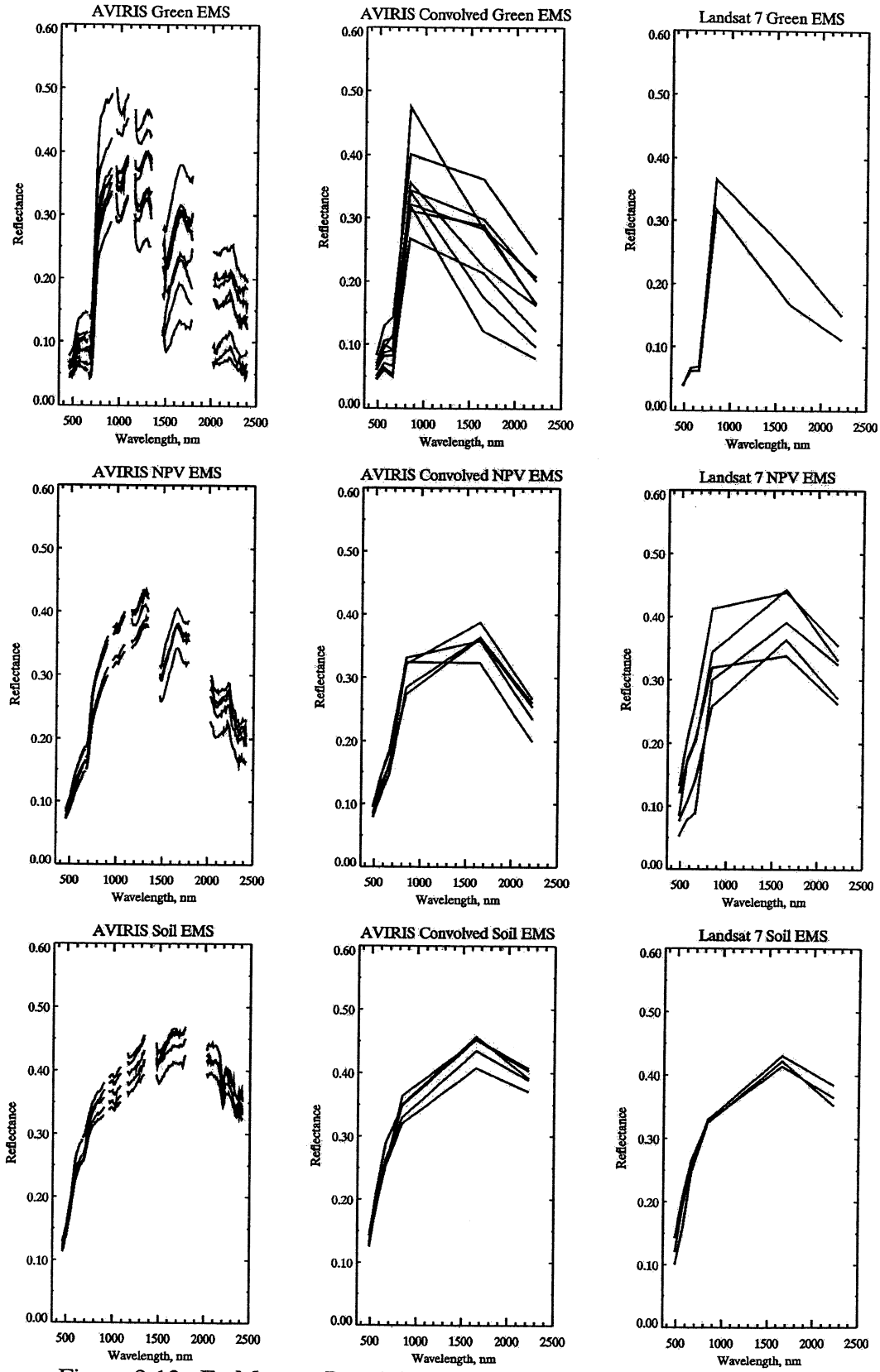

Figure 3.12. Ft. Morgan Run 2 Scene 9 endmember (EMS) bundles.

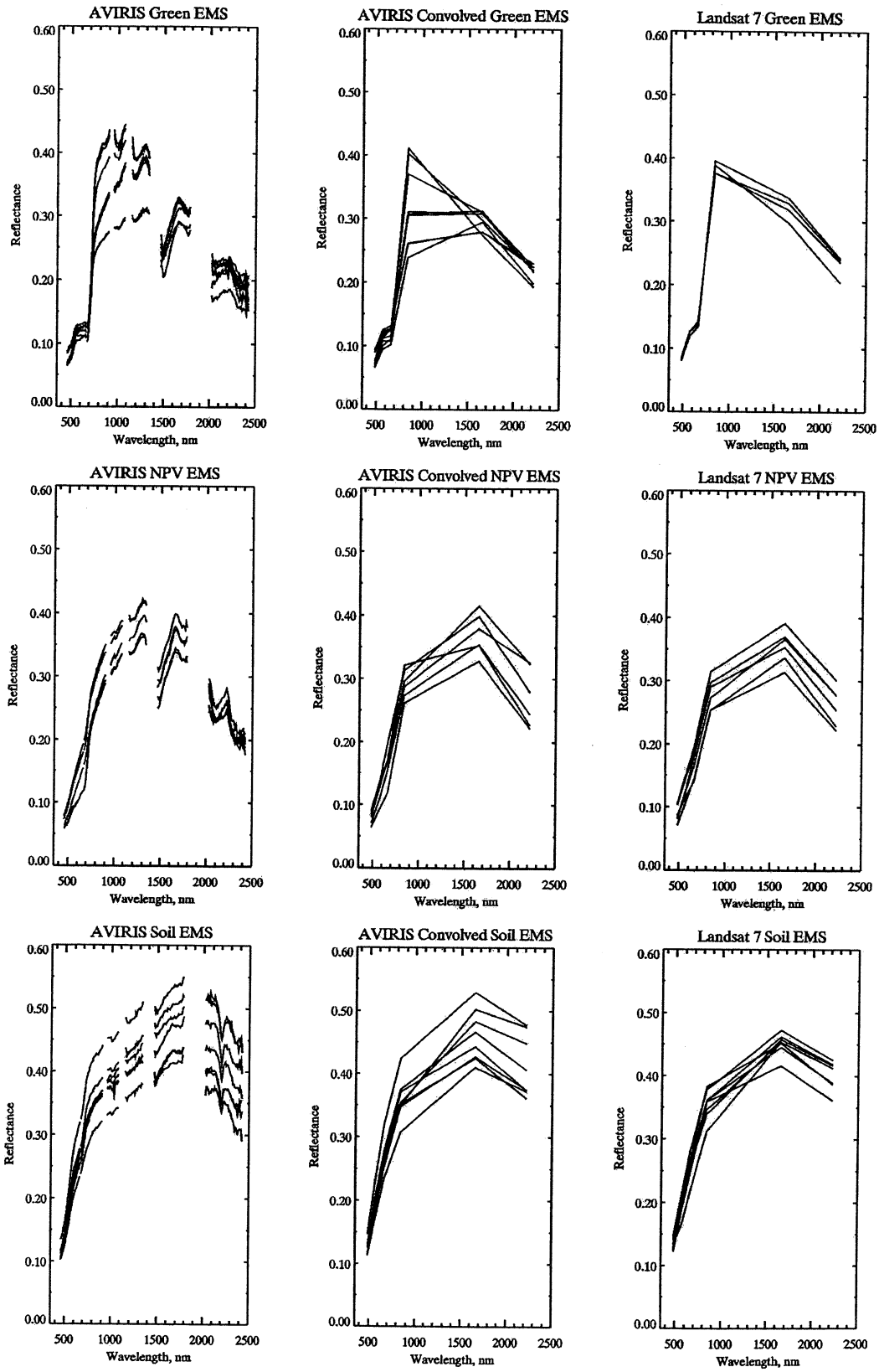

Figure 3.13 Ft. Morgan run 2 scene 10 endmember (EMS) bundles.

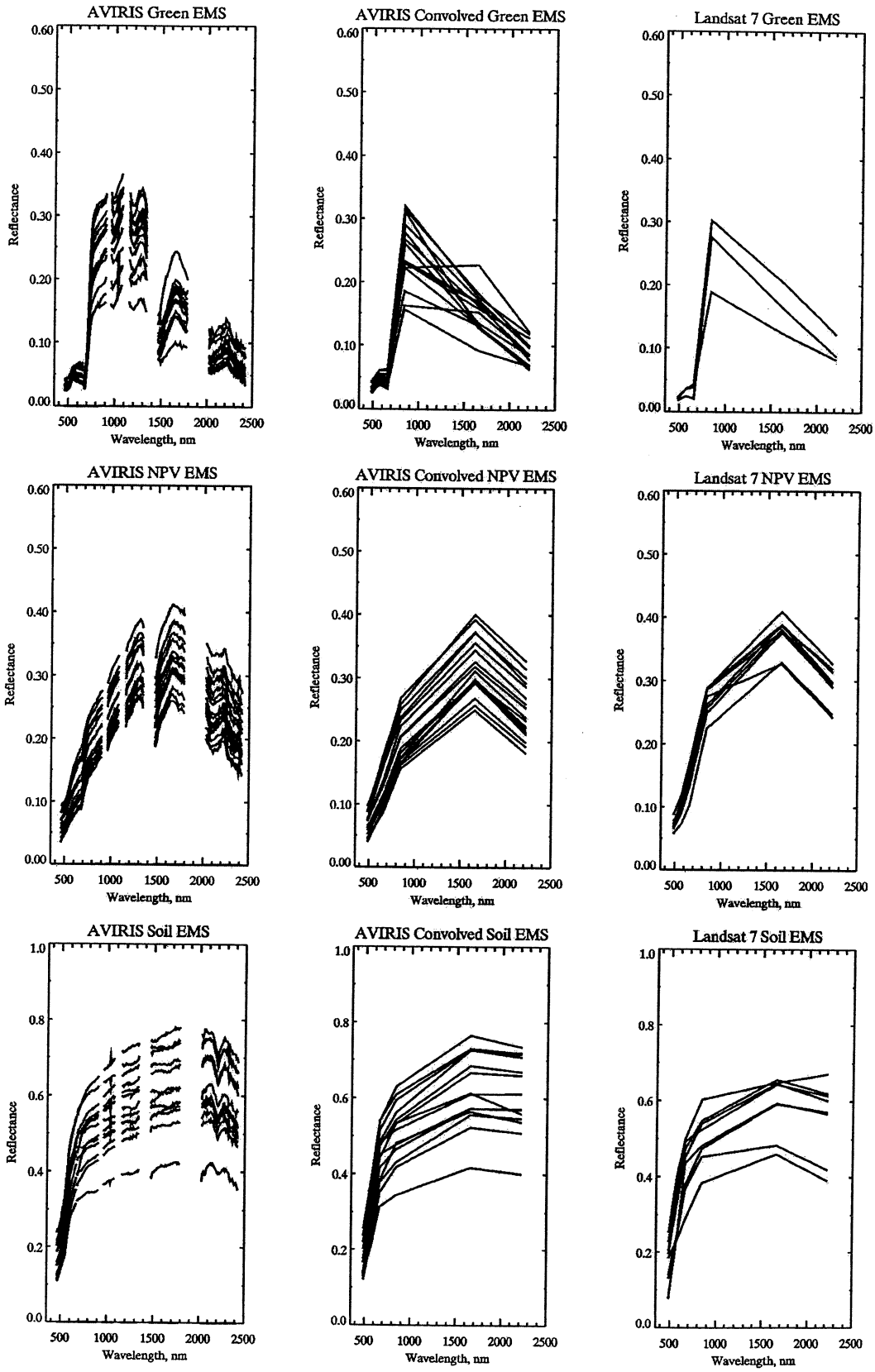

Figure 3.14. Logan run 2 scene 2 endmember (EMS) bundles.

Endmember Bundle Variability

Both the Ft. Morgan and Logan areas have rolling terrain. The irradiance on these surfaces varies with the cosine of the incident angle. A simple sensitivity study to look at the effect of an undulating surface (in these situations, sand dunes) with long wavelength features of 100+ meters and 5-10m in amplitude was performed to observe the variability that topography can introduce to the endmember bundles, see figure 3.15 and table 3.1.

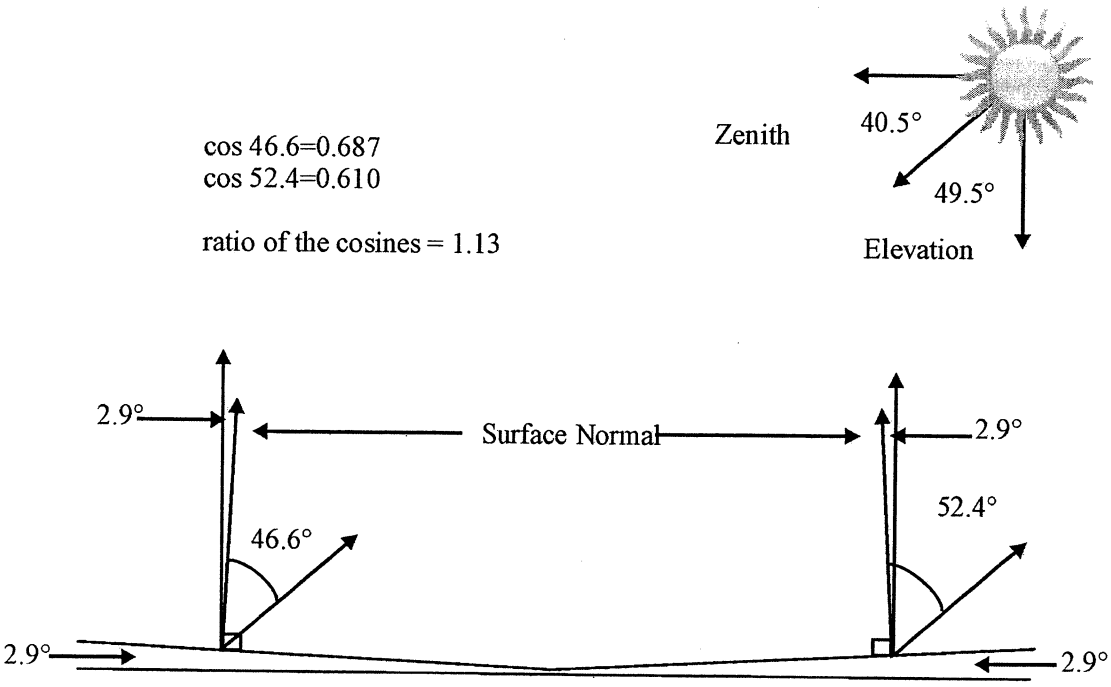

Figure 3.15. Schematic of the Ft. Morgan AVIRIS scenes used in this study. The 2.9° angle is the slope of the surface for a 5m high and 100m long surface feature. The ratio of the cosines shows there is a 13% variability in the irradiance on the dune facing toward the sun (46.6° angle) and the dune facing away from the sun (52.4° angle).

Table 3.1

	Zenith	Elevation	Slope	incident angle (toward sun)	incident angle (away from sun)	Ratio of the cosines of the incident angles
Ft. Morgan AVIRIS	40.5	49.5	2.9	46.6	52.4	1.13
Ft. Morgan Landsat	26.6	63.4	2.9	60.5	66.3	1.23
Logan AVIRIS	50.4	39.6	2.9	36.7	42.5	1.08
Logan Landsat	41.8	48.2	2.9	45.3	51.1	1.11

As shown in table 3.1, the topography of a region at a given solar elevation can affect the irradiance incident on the surface by 8-23 % as illustrated in this simple situation of using a constant slope. In reality the surface is far more complex with the solar azimuth, inherent BRDF properties of surface materials, sensor-scan geometry, and atmospheric conditions contributing to albedo of the surface.

Linear Spectral Unmixing

Unconstrained linear spectral unmixing is the approach used in this study to compute relative abundances of surface materials. Linear spectral unmixing, as explained in the previous section, assumes that the resulting spectrum of a pixel is a linear combination of a given group of endmembers. Unconstrained means that the fractions of a given pixel should not be forced to sum to one and be greater than zero. By not forcing the data to meet the feasibility constraints, the data themselves can better be evaluated to determine if a particular set of endmembers or method of mixture analysis is functioning properly.

Selecting the appropriate endmember combination to unmix a pixel or group of pixels can be very time consuming. All of the pure surface materials contained in the pixel being unmixed must be included in the endmember spectra for feasible

unmixing results to be produced. Bundling of endmembers incorporates the natural variability of vegetative surfaces to provide realistic cover fractions instead of unmixing with several spectra that only include the variablity of one pure image pixel (see previous section for discussion on bundling).

One method that incorporates endmember bundles was developed by Asner and Lobell (2000). This method, called AutoSWIR, uses a Monte Carlo algorithm to randomly select endmembers from endmember bundles and then perform unconstrained linear spectral unmixing with the endmembers selected for the pixel it is evaluating. AutoSWIR performs this unmixing with random endmembers for a user determined number of iterations. After the final iteration for a pixel it computes a mean fraction for each cover type. A standard deviation of the fractions computed for each pixel is also computed and provides a confidence interval for each pixel, see figure 3.16 (Asner and Lobell, 2000).

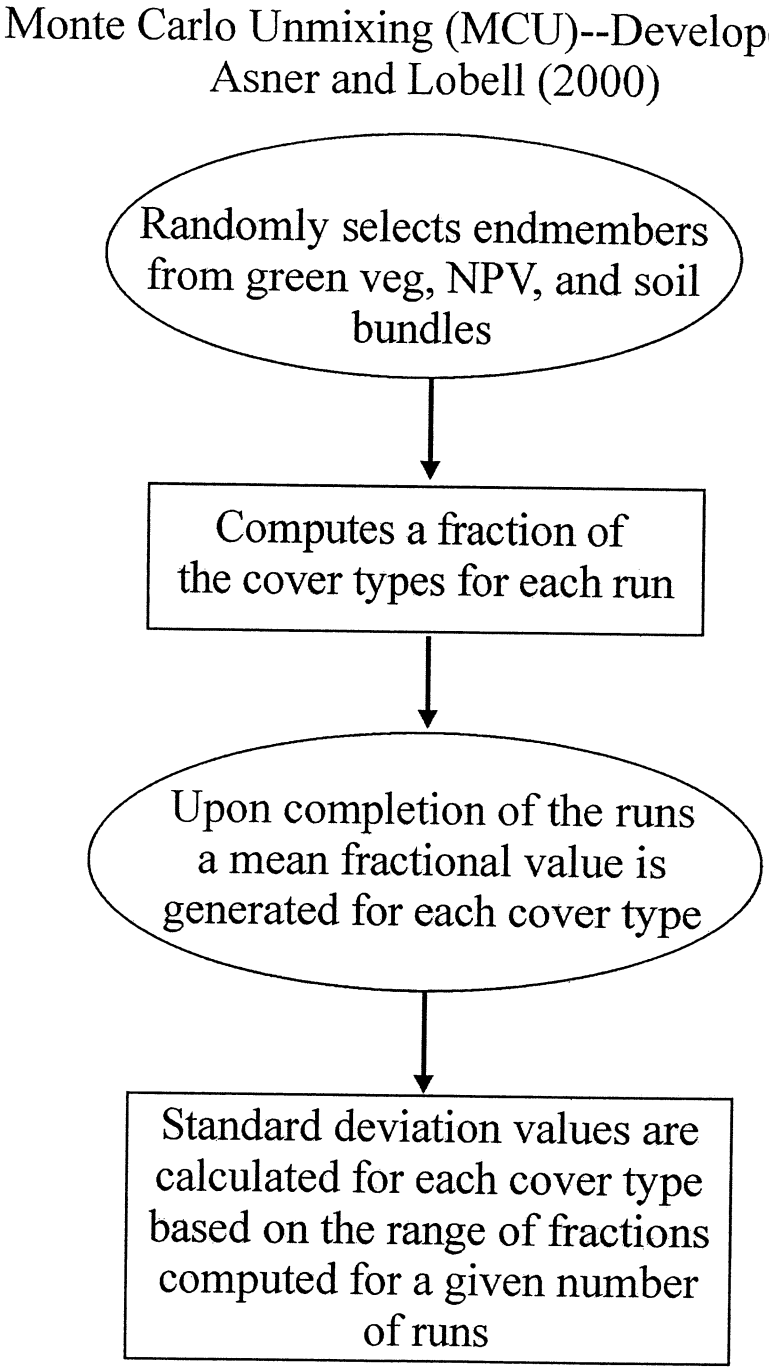

Figure 3.16. Schematic of Monte Carlo Unmixing.

The method developed by Asner and Lobell (2000) is more suited for studies with high spectral resolution, such as hyperspectral data, as it uses a subset of the SWIR 2 (2100-2400 nm) region of the solar reflected spectrum for the use in the endmember bundles. The spectral subset in this region is then tied to a user defined

wavelength to remove the influence of albedo. The spectra being unmixed are also tied in this manner. The spectral differences of soil, green vegetation, and NPV are most separable in the SWIR 2 region given the water absorptions in green plants, lignin and cellulose features in NPV, and clay mineral absorption features in soils. One of the strengths of AutoSWIR is in the low variability of the tied endmember bundles, resulting in lower standard deviations from the mean fractions (Asner and Lobell, 2000, Lobell et al, in review).

Detailed Description of AutoSMA

The method applied in this study, called AutoSMA, uses full spectrum Monte Carlo Unmixing and has been developed by Asner et al (in review) for better suitability in unmixing Landsat data. This method involves unmixing with full spectrum endmembers (with atmospheric water bands and "noisy" bands removed) to better work with Landsat data, which cannot be tied in the SWIR2 region. Using the full spectrum to perform mixture analysis limits the use of the spectral shape in mixture analysis as some of the variation in the endmember bundles can be attributed to albedo. AutoSMA is written in the Interactive Data Language (IDL)™, see table 3.2 for a detailed description of the code.

Table 3.2. AutoSMA Detailed description

Code Input	• Full spectrum endmember bundles (bad bands removed). • AVIRIS (bad bands removed) and/or TM scene. • User defined number of runs.
Processes in the Code	• Sorts endmember bundles according to the value of the last band. • Takes a subset of the endmember bundles containing between 10-90% of the variability. • Generates random sequence of endmember combinations and performs Singular Value Decomposition (SVD) on each pixel using the random combination of endmembers for the appropriate run. • Removes the upper and lower 10% of fractions for each pixel to remove outliers (added to the code by the author). • Computes a mean and standard deviation for the range of fractions for each cover type, for each pixel. • Computes a recombination spectrum for each pixel using the endmembers and the fractions generated for each run (added to the code by the author).
Code Output	• Mean fraction image (upper and lower 10% of values removed). • Standard deviation image showing the standard deviation of the means for each pixel (again with upper and lower 10% removed). • Recombination image generated using all fractions

Asner et al, in review.

The number of runs used in the code is based upon the principle that the distributions of fractions for each endmember is normal and converges on a mean, see figure 3.17 (Asner and Lobell in press; Lobell et al, in review). 50 runs was deemed the point where the means converge sufficiently; the fractions and standard deviations only deviated slightly after that point.

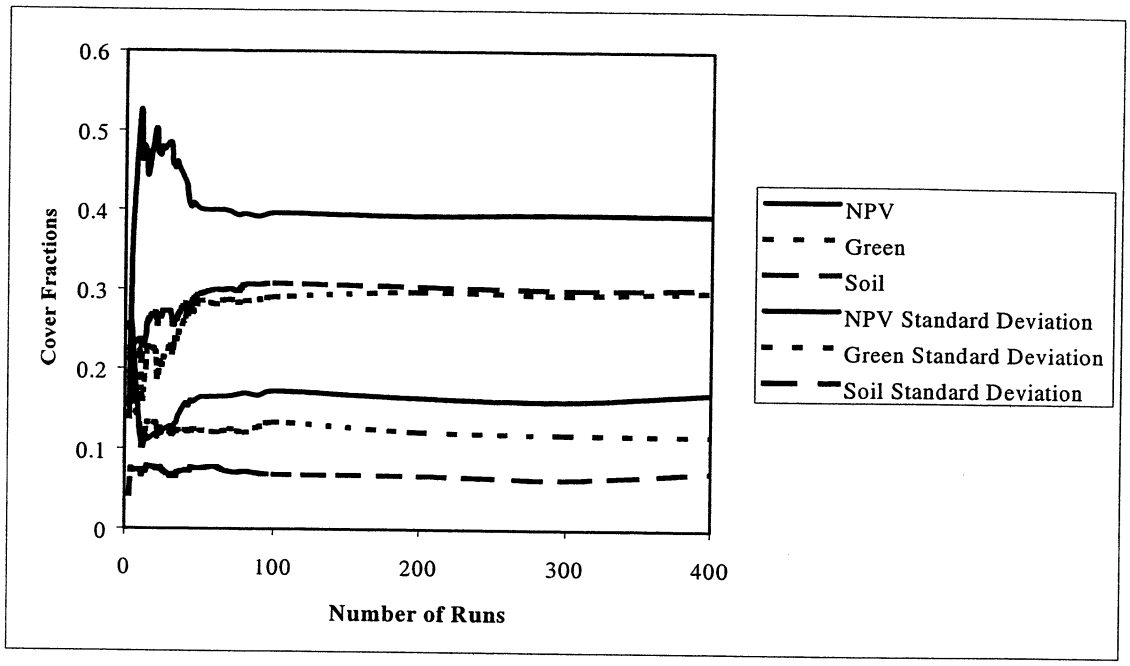

Figure 3.17. Mean and standard deviation of cover fractions of Monte Carlo Unmixing.

Following the completion of AutoSMA on Landsat 7 and AVIRIS images, the mean and standard deviation images are viewed and regions of interest selected. For each of these regions ranging in size from 100 pixels to 400 pixels, a mean fractional cover for each cover type is produced as well as standard deviations for the regions for each cover type. These regions were also selected for the corresponding geocorrected AVIRIS image. These data were then plotted against each other and slopes, offsets, and correlation coefficients were generated for each cover type.

Three AVIRIS scenes were used in this study of vegetation on the High Plains. Two from the Ft. Morgan lines and one from the Logan line. The Ft. Morgan scenes used are sub-scenes of run 2 scene 9 and run 2 scene 10, hereafter referred to as FM0209 and FM0210. The Logan sub-scene used is run 2 scene 2 of the Logan, NM line. Sub-scenes were used so that cultivated fields were not included in the

dimensionality of the imagery as well as to only include landscapes pertinent to this study.

Chapter 4

Results

Spectral Characterization

This is a study to assess the ability of Landsat 7 data to map sparse vegetation using fieldwork and AVIRIS imagery as a basis of comparison. Ancillary field data, such as spectral characterization at the Ft. Morgan site, and line transect measurements, collected to assist interpretation the data raised questions about the quality of the field data collected as well as resulting imagery interpretation.

Spectral characterization was performed only at the Ft. Morgan site. The Logan field site is distant and performing measurements the day of the flight was not logistically possible. The spectral characterization of the Ft. Morgan vegetation site was performed beginning at 10 a.m. the morning of the AVIRIS and Landsat 7 overflights, with AVIRIS flying over the site at approximately 10:11 am MDT. At the beginning of the measurements, the computer of the spectrometer froze several times and needed to be rebooted. The spectra that were recorded were very noisy, especially in the SWIR 2 region. Optimization of the spectrometer was performed several more times, but with no improvement of the quality of the spectra. It was

determined to proceed with the measurements since there was only one opportunity to get the same solar illumination, vegetation condition and orientation as AVIRIS was imaging, see figure 4.1. There is reasonable agreement among the spectra. The ASD spectra, although noisy, when resampled to AVIRIS wavelengths and a mean taken, were acceptable. The disparities between the field collected mean spectrum and image derived mean spectrum can be associated with improper image registration (GPS points were differentially corrected) and the inability to locate GPS measurements with .5m accuracy in a 17.2m and 15.6m pixel. The PSF of both instruments, field spectroscopic techniques e.g., pace, distance between transects, and transect orientation relative to the scan angle of AVIRIS, can additionally affect the agreement of the spectra.

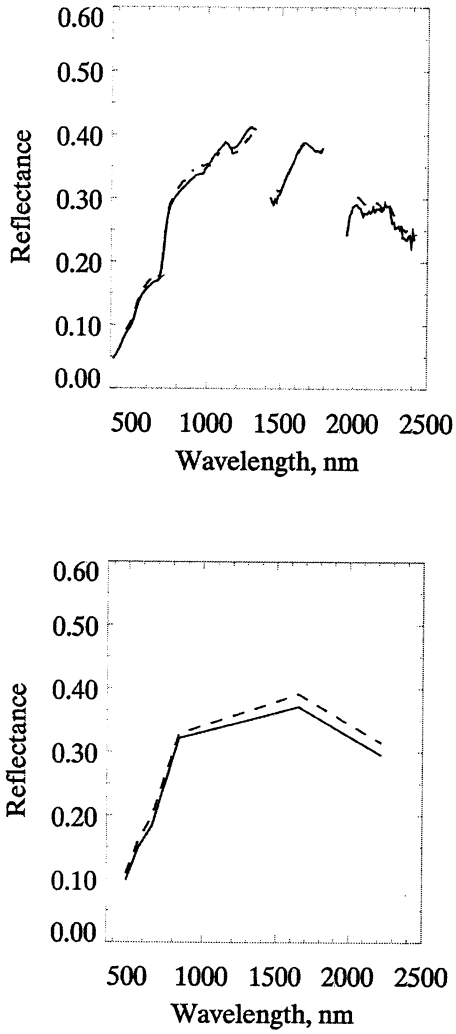

Figure 4.1. Ft. Morgan vegetation study site spectra. Dashed lines are mean AVIRIS and Landsat 7 spectra. Solid lines are the ASD mean field spectrum convolved to the respective sensor.

Unmixing Results, Ft. Morgan

The AutoSMA results for two of the Ft. Morgan scenes that contain stabilized sand dunes yielded physically, and spectrally feasible results. Initial methods using one invariant group of endmembers for one area yielded unfavorable results. Monte Carlo Unmixing with the program AutoSMA (Asner et al, in review) allowed for the

maximization of endmembers variability with the incorporation of endmember bundles.

The fractions for the study area used in the FM0209 sub-scene did not correlate well to the fractions counted in the field with the line intercept method, see table 4.1. The standard deviation does not place the MCU derived fraction within the field counted values. See Discussion for sources of error with field measurements and remotely sensed measurements.

Table 4.1, Ft. Morgan study site Field data and AutoSMA results

	Field Fractions (%)	AVIRIS	Standard Deviation	Landsat 7 with AVIRIS Endmembers	Standard Deviation	Landsat 7 Endmembers	Standard Deviation
NPV	8.5	34.5	13.4	32.2	16.7	27.0	18.2
Green	70.00	17.9	9.8	13.0	9.2	14.9	5.0
Soil	21.5	48.5	7.2	53.9	10.0	60.5	14.0
Total	100.00	100.9		99.1		102.4	

The AVIRIS AutoSMA results for FM0209 are very well correlated to the AVIRIS endmember bundles unmixing Landsat 7 sub-scene, see figure 4.2 and Appendix A for all cover fractions. The standard deviations computed are smallest for the soil fraction. The standard deviation places the AVIRIS fraction within the standard deviation calculated for unmixing Landsat with AVIRIS endmember bundles (see table 4.2). This agreement indicates that AVIRIS endmembers can be used successfully to unmix Landsat 7 data, even if the fractions are not the same. This is a powerful tool in using the spectral advantages of AVIRIS for multispectral data.

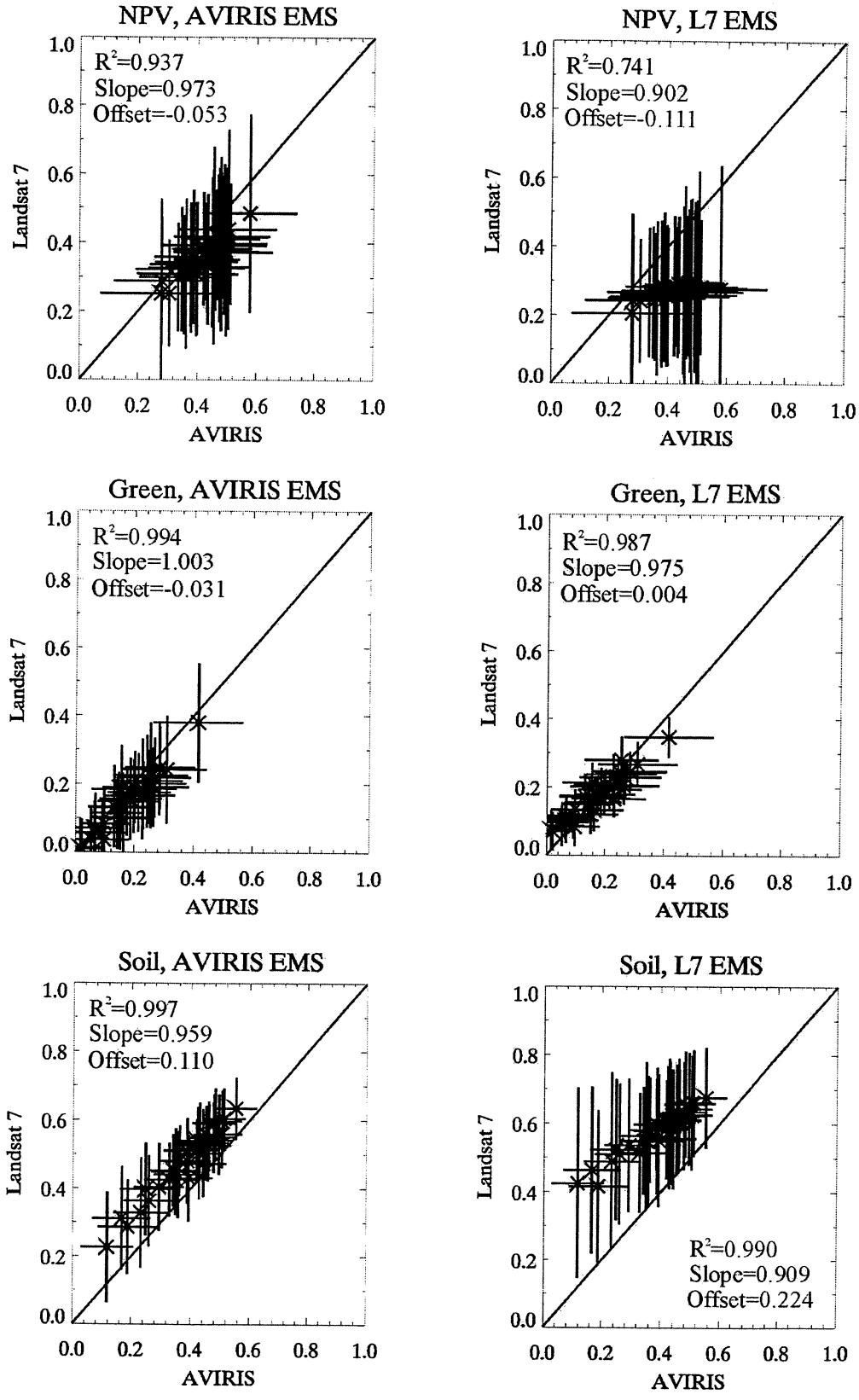

Figure 4.2. FM0209 cover fractions derived with AutoSMA.

Table 4.2. Soil fractions and standard deviations for FM0209.

	AVIRIS fractions		TM w/ AVIRIS EMS		L7 EMS fractions	
region	soil frac	St. Dev	soil frac	St. Dev	soil frac	St. Dev
1	0.461609	0.069321	0.549879	0.096685	0.61989	0.137783
2	0.456539	0.078608	0.525475	0.103942	0.609581	0.149449
3	0.292117	0.083313	0.404505	0.127792	0.536739	0.194133
4	0.476592	0.076159	0.550125	0.103163	0.622317	0.157997
5	0.552159	0.070435	0.634187	0.090084	0.675765	0.146588
6	0.48222	0.072374	0.590317	0.102996	0.655621	0.153789
7	0.386101	0.077177	0.511161	0.093211	0.597283	0.132241
8	0.440634	0.076153	0.531309	0.094233	0.602507	0.149112
9	0.505079	0.065738	0.596908	0.089514	0.660809	0.137639
10	0.427446	0.0819	0.502978	0.132855	0.599447	0.18995
11	0.392934	0.078976	0.430635	0.127007	0.549817	0.193187
12	0.494086	0.079242	0.558497	0.116809	0.642162	0.164086
13	0.387555	0.07972	0.480703	0.125199	0.578366	0.184228
14	0.34095	0.081766	0.453343	0.104748	0.549543	0.156142
15	0.419147	0.078933	0.512386	0.091564	0.582986	0.144472
16	0.259424	0.084343	0.364133	0.133449	0.510669	0.204944
17	0.426097	0.076281	0.518352	0.099056	0.592199	0.165816
18	0.247317	0.087995	0.398341	0.135715	0.523424	0.206155
19	0.362776	0.073507	0.481302	0.103199	0.581174	0.152561
20	0.421837	0.078167	0.540627	0.09824	0.610932	0.157079
21	0.511115	0.072255	0.604339	0.088251	0.658825	0.154778
22	0.166097	0.098717	0.312111	0.151924	0.463227	0.243797
23	0.430337	0.074681	0.537048	0.114213	0.609871	0.171331
24	0.459334	0.077232	0.54098	0.113114	0.625111	0.16375
25	0.45161	0.07434	0.533288	0.108787	0.61042	0.16148
26	0.356762	0.081786	0.441285	0.127191	0.547903	0.1902
27	0.47692	0.074477	0.591443	0.084525	0.633636	0.139271
28	0.504452	0.069112	0.559312	0.098746	0.6248	0.159355
29	0.439247	0.07282	0.525867	0.106743	0.590188	0.168403
30	0.349482	0.083719	0.449656	0.126776	0.563746	0.214929
31	0.442217	0.076777	0.472863	0.096634	0.555643	0.146612
32	0.11694	0.090167	0.227147	0.162777	0.424694	0.277798
33	0.232438	0.093772	0.329068	0.161796	0.489287	0.25937
34	0.327849	0.085204	0.425897	0.10874	0.514312	0.174362
35	0.186793	0.099886	0.286846	0.138644	0.415985	0.223238

The fractions derived with Landsat 7 endmember bundles for FM0209 are well correlated with the AVIRIS fractions, but the standard deviations, especially for the lower fractions, are large. The standard deviation that is produced as a result of

AutoSMA serves to show the variation in endmembers used as well. Very similar endmembers are going to have similar fractions when unmixed. Large standard deviations indicated a wider range of fractions were computed for each pixel. The standard deviations calculated using AVIRIS endmember bundles are almost always substantially smaller than those of the Landsat 7 endmember bundle derived fractions, but the larger of the two must be used in estimating the error. These results indicate that unmixing with Landsat 7 can provide comparable results to the AVIRIS data, but there is a tradeoff in the large range of error that is associated with the Landsat 7 unmixing. By using AVIRIS endmembers to unmix the Landsat data, the fractions derived with AVIRIS endmembers can be directly related to AVIRIS fractions. The NPV and green fractions are well correlated, but with greater standard deviations than the soil endmember, overall. Using the Landsat 7 endmember bundle overestimates the soil cover, but again, the standard deviations of the Landsat soil fractions are large enough to include the AVIRIS fractions within the range of error which is as much as ±15% the mean for the soil endmembers.

Fraction images produced with AutoSMA support visual image interpretation with the mapping of the fractions, see figure 4.3. These images provide a clear representation of the fractions and highlight the offsets that are produced with the linear regressions in figure 4.2.

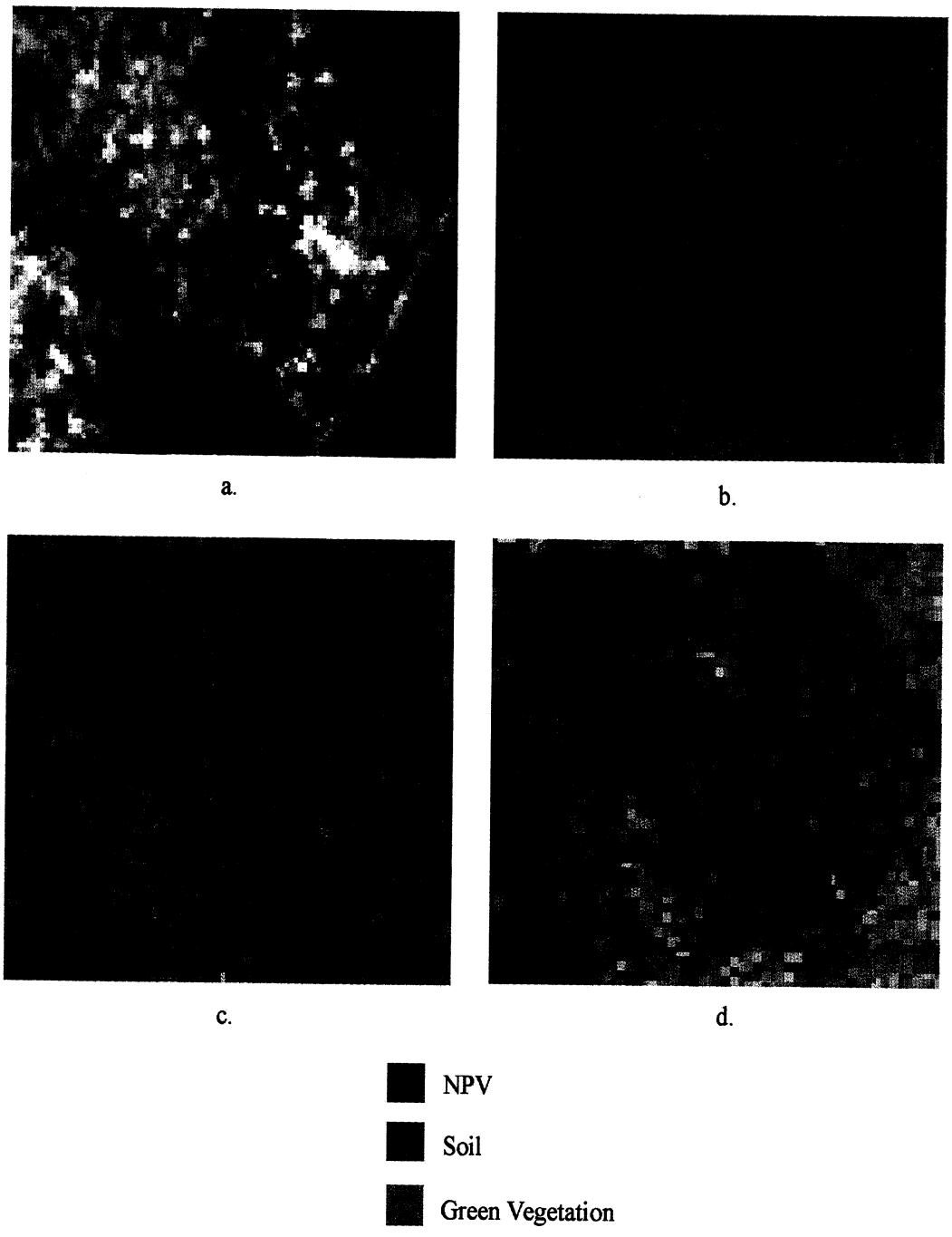

Figure 4.3. Fraction images from FM0209; all images have been stretched with a 2% stretch. a. CIR image of the of FM0209 sub-scene, b. fraction image of the AVIRIS scene, c. fraction image of Landsat 7 with Landsat 7 endmembers, d. fraction image of Landsat 7 using AVIRIS endmembers. Note the differences in the AVIRIS fraction image (b) and the Landsat image (d) using AVIRIS endmembers. The Landsat image (d) shows greater concentrations of soil, which is mathematically shown on figure 4.2 with the offset of the regressed line being greater than zero for comparing AVIRIS and Landsat 7 using AVIRIS endmembers.

Recombination spectra are produced for every pixel that is unmixed. These recombination spectra are calculated by taking the fractions derived from the randomly chosen spectra and multiplying them by the spectra used in unmixing for each run. A spectrum is recreated for each pixel for each run, these spectra are added together and divided by the number of runs. The resulting spectrum can then be compared to the original. The fractions derived do not present a unique solution, but are an indicator that the algorithm is producing feasible results, see figure 4.4 for recombination spectra from FM0209.

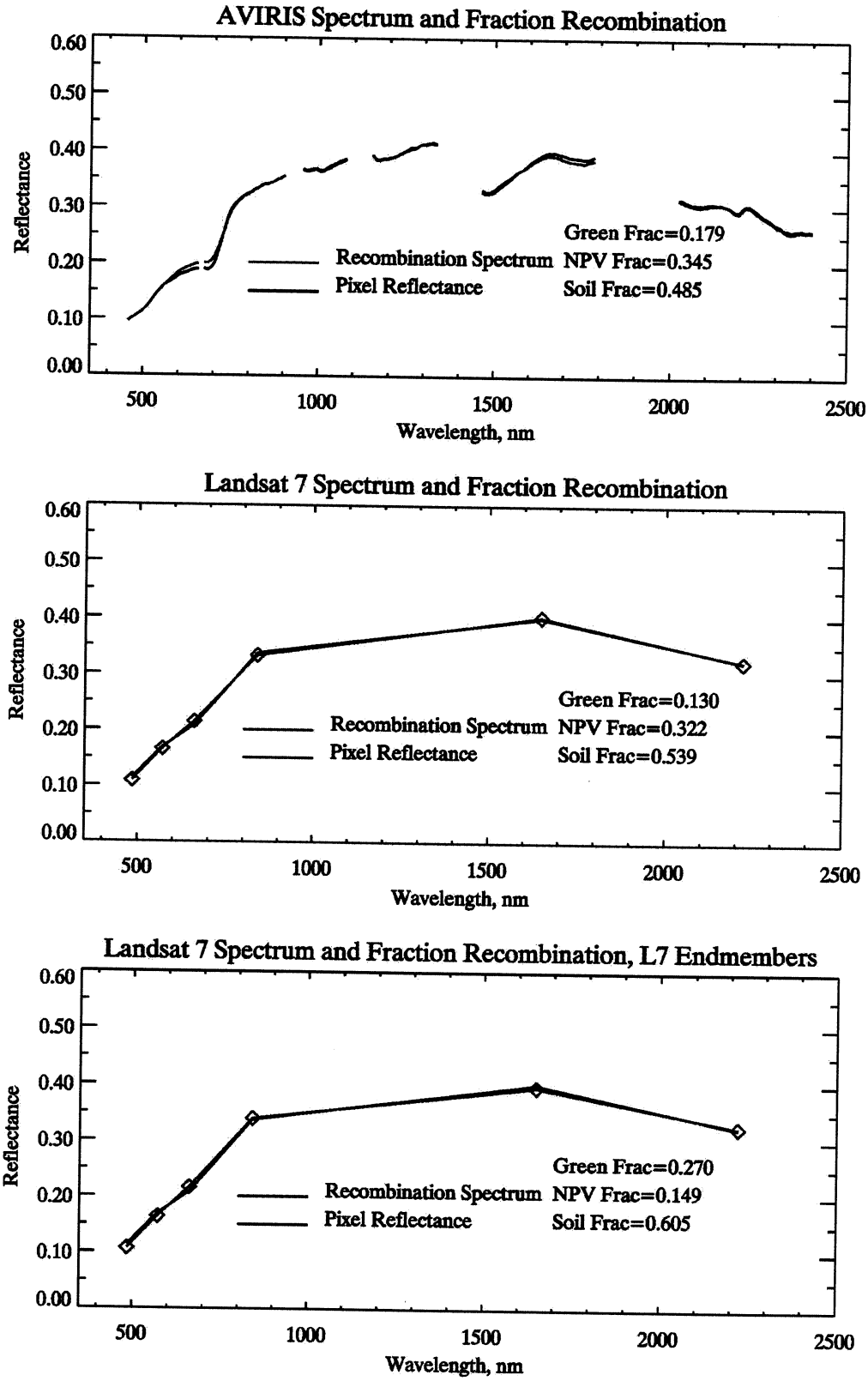

Figure 4.4. Recombination spectra and fractions from vegetation study site in FM0209.

A region on the stabilized dunes in FM0210 was chosen and Monte Carlo Unmixing (Asner and Lobell, 2000; Asner et al in review) performed. This site is geographically larger than FM0209. The correlations of the fractions with FM0210 were similar to the correlation of the fractions derived with FM0209. The plots of FM0210 fractions derived with Landsat and AVIRIS endmember bundles show very good correlation, see figure 4.5. Although the green fractions and NPV fractions are well correlated, the standard deviations are broad enough that the points are not very precise and are not ideal for measuring fractional abundance. The soil fractions at this location have a smaller range of standard deviations than for the NPV and green vegetation.

Unlike FM0209, the mixture analysis with Landsat 7 endmembers underestimates the soil fractions, see figures 4.5 and 4.6. Since the endmembers that can be resolved in the Landsat 7 imagery are spatially and spectrally different from AVIRIS, the fact that the fractions are offset in a different way is not surprising. In expanding the mixture analysis to include endmembers derived from Landsat 7 there is a change in the quality of endmembers that can be found due to pixel size, spectral sampling, and state of the vegetation cover.

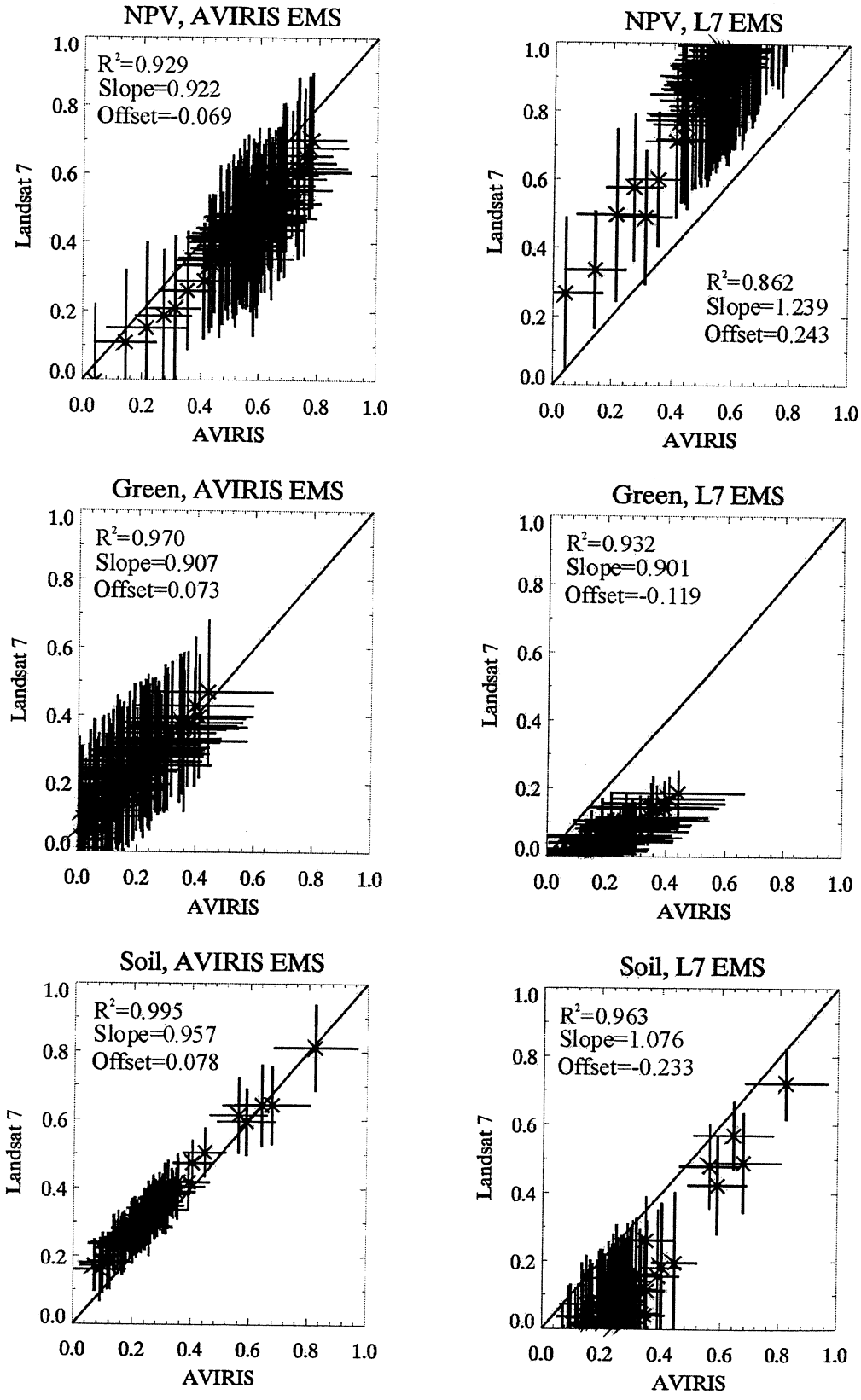

Figure 4.5. FM0210 AutoSMA results.

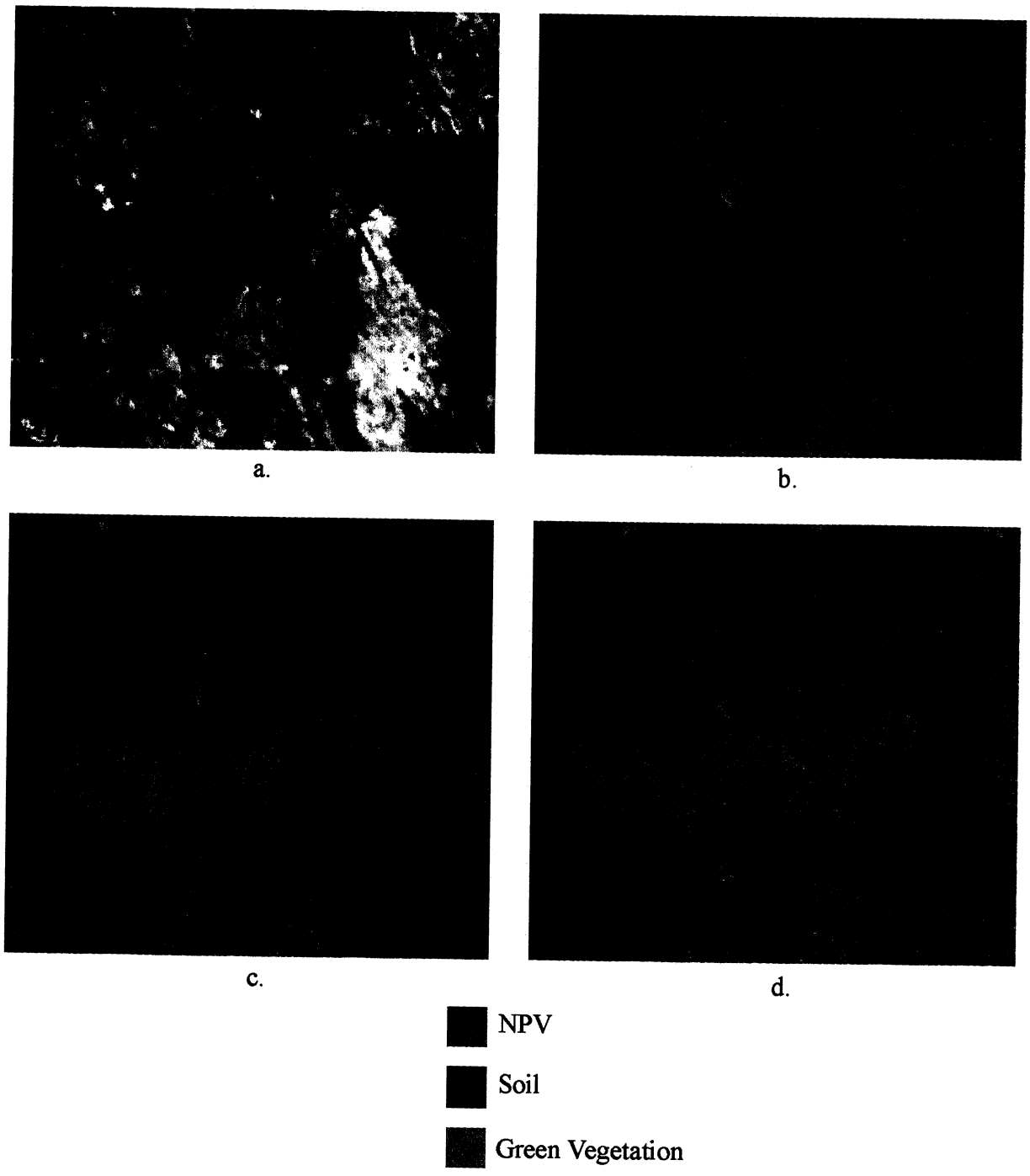

Figure 4.6. FM0210 fraction images, all images have been stretched with a 2% stretch. a. AVIRIS CIR image, b. AVIRIS fractions, c. Landsat 7 endmember fractions, d. Landsat 7 fractions derived with AVIRIS bundles. The similarities in the images are indicative of the high correlation and minimal offsets of all the fractions for this scene, see figure 4.5.

Combination of FM0209 and FM0210 Endmember Bundles

The sub-scenes used for the Ft. Morgan area are approximately 10km apart. FM0209 had not been grazed the year prior to the overflight. FM0210, though not visited, is under different ownership than FM0209. From fence line patterns and regions dominated by NPV, the conclusion that this area has been recently grazed is logical. Though the land in the FM0210 scene has been managed differently, which would result in different green vegetation and NPV spectra than those selected in FM0209, the soil is the same type for both areas. The endmember bundles for FM0209 and FM0210 were combined to determine if using this endmember combination would produce similar fractions of soil, see figures 4.7 and 4.8.

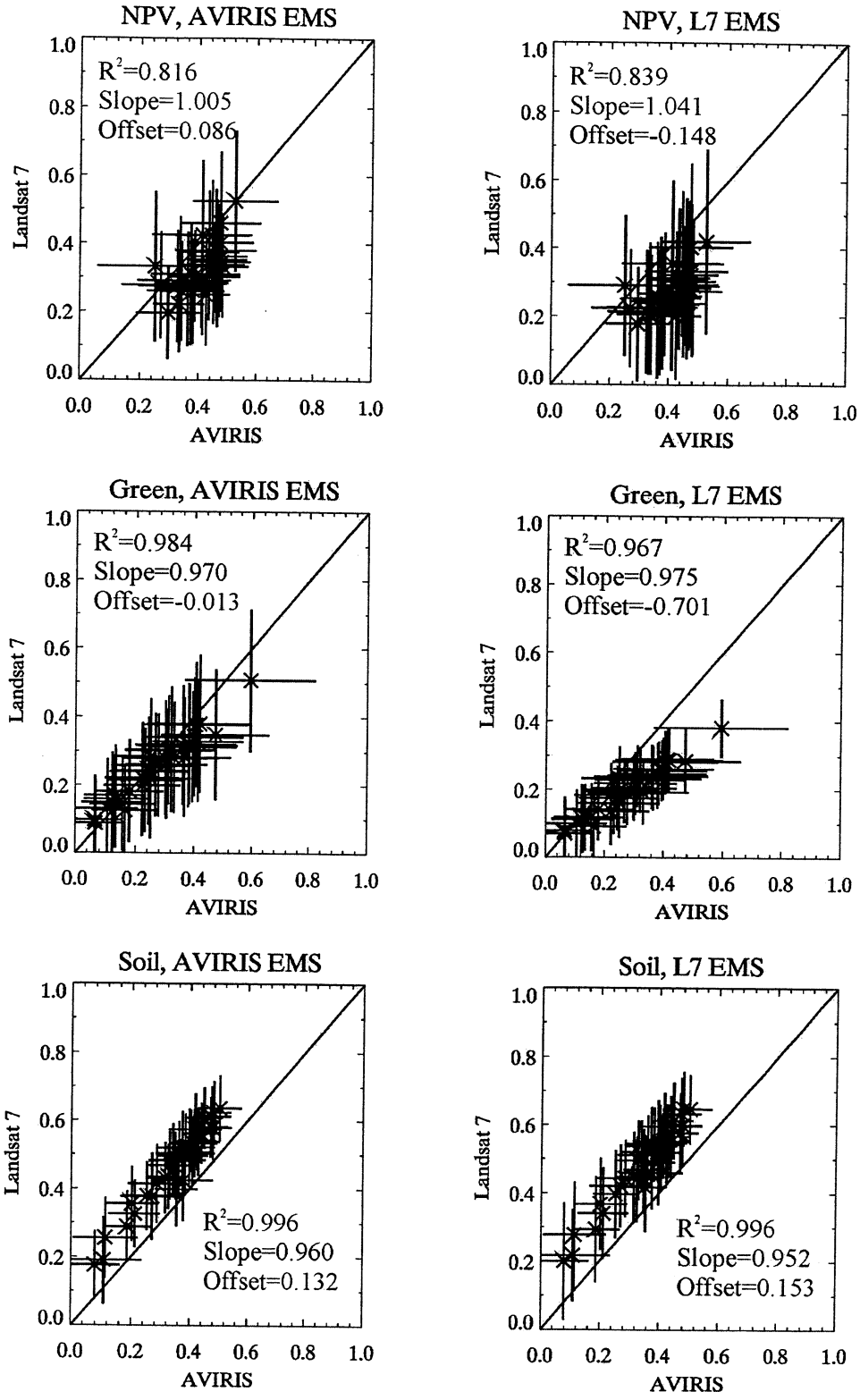

Figure 4.7. FM0209 results for combining the endmember bundles from FM0209 and FM0210.

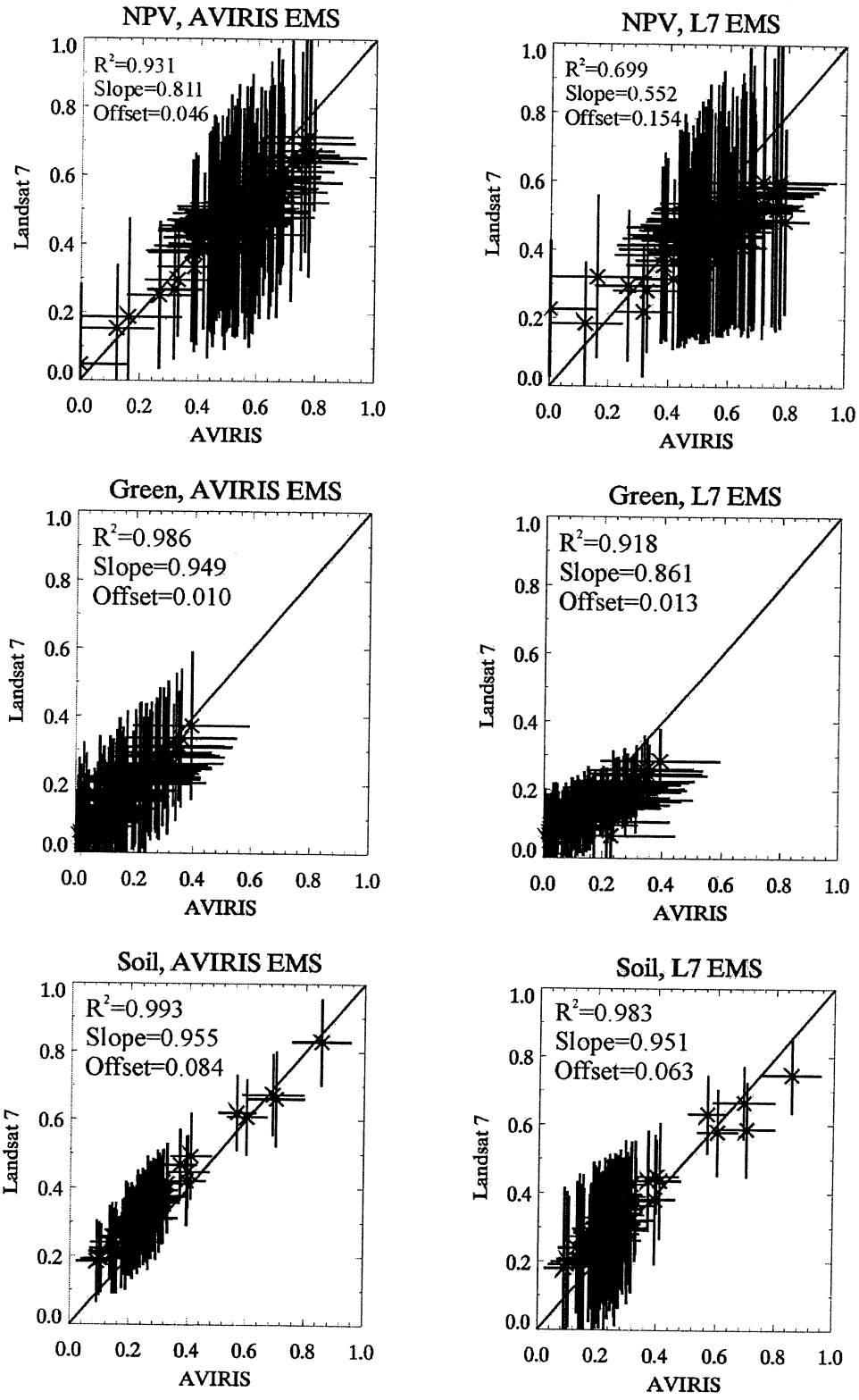

Figure 4.8. FM0210 results for combining the endmember bundles from FM0209 and FM0210.

The soil fractions are the most highly correlated of the combined bundle results as well as have the smallest standard deviations. The statistics that are produced are dependent upon the spectra in the bundles. By combining the bundles, there is more variability in the green vegetation and NPV bundle since there are two different forms of land management, but not as much in the soil bundle since the two scenes are on the same soil type (USDA 1968). The large standard deviation for the NPV fractions for FM0210 is attributable to the wider range of NPV spectra in the bundles. The soil fractions for the Landsat 7 FM0209 sub-scene using Landsat 7 derived endmembers have a smaller standard deviation than the soil fractions using only the endmembers from FM0209. This change can be associated with there being only three soil spectra in the bundle used to unmix FM0209, but the combined bundle had 9 spectra, and more variability. The three used by the Landsat 7 FM0209 image are very similar and may not be including the surface variability well enough. By combining the bundles and achieving very similar soil fraction to those with the individual bundles, the green vegetation and NPV bundle quality are not significant in mapping soil cover, provided the soil bundles are appropriate for the region.

Logan, NM

Because of the timing of the flight, it was not possible to make ground measurements the day of the flight. Fortunately, the large sand dunes serve as spectrally invariant targets for surface reflectance measurements. The location the vegetation was measured using the line intercept method was a north facing slope of the dune (the south facing slope had nothing to measure). Vegetation measurements and calibrations measurements were made on October 14, 1999. At this time of year

the vegetation that was on the dunes was predominately NPV. These measurements, as opposed to the Ft. Morgan measurements, are in a relatively simple system since there is little to count. The author has more confidence in the vegetation counted here than at the Ft. Morgan vegetation due to the complexity of the Ft. Morgan landscape. In comparing the vegetation measurements recorded at Logan to the MCU results for this area, there is significantly more cover derived for these regions with AutoSMA, see Table 4.3.

Table 4.3. Logan, NM Vegetation study site results

	Field Fractions (%)	AVIRIS	Standard Deviation	Landsat7 with AVIRIS Endmembers	Standard Deviation	Landsat 7 Endmembers	Standard Deviation
NPV	7.3	33.9	14.8	65.02	13.8	49.2	27.5
Green	2.0	5.8	7.2	20.0	6.9	-6.5 (left out)	31.5
Soil	90.7	55.1	7.4	37.9	9.0	45.6	17.2
Total	100	94.8		122.92		94.8	

*Note the soil fractions with AVIRIS and Landsat 7 using AVIRIS endmembers are not within the standard deviation of each other, the nature of the site being in a boundary situation is to blame in skewing the mean.

The fractions derived from the AVIRIS endmembers used with the AVIRIS data and Landsat 7 endmembers sum to 94.8%, indicating that the endmember bundles have not encompassed the variability on the surface. The greater than 100% result using the AVIRIS endmember to unmix the Landsat 7 data indicates that the mixture in this region is beyond the mixing surface of the mixing simplex.

The PSF of the sensors plays a large role in the excess of NPV and green vegetation in the mixing results compared to the field measured values. As shown in figure 4.9 the contact between 100% cover and sparse vegetation is very distinct. With 25-30% of the signal for a pixel coming from out of the pixel geometric area, this effect could strongly influence the resulting spectra and hence the poor

correlation with the field measurements of the vegetation. Another source for the disparity in the field and image derived fractions could be difference in the date the images were collected and the date of the fieldwork, which was 15 days after the images were acquired. Different branch orientation, illumination conditions, sand movement covering vegetation, and live and dead fractions at this time could all play a role in the disparities.

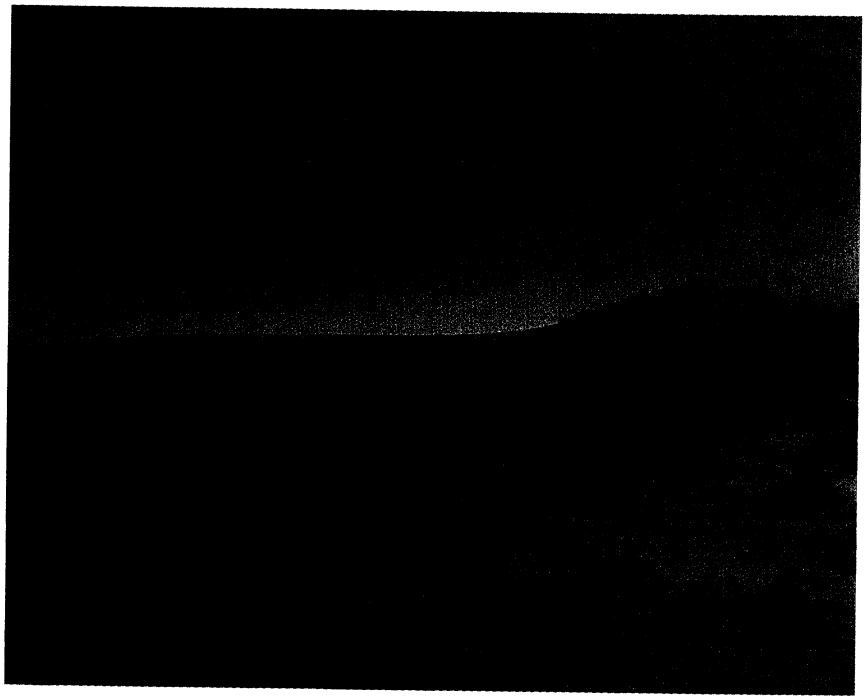

Figure 4.9. Sand dune near Logan, NM. Calibration measurements performed on crests of dune, vegetation transect measurements included crests in region counted. The left center part of the image shows significant cover next to areas of very sparse vegetation.

The comparison of unmixing the Landsat data with AVIRIS endmember bundles and unmixing the Landsat 7 data with Landsat 7 endmember bundles yielded highly correlated fractions for each cover type, see figure 4.10. The fractions were not always physically feasible with some being greater than one and less that zero. Regions of soil that are greater than one can be assumed to be pure soil and indeed

there are areas within this scene that only contain pure soil, see figure 4.11. The more directly illuminated south facing slopes (which is where the soil fractions are greater than one), could also be responsible for the above-one fractions with NPV as well, as this region is very hilly. The standard deviations of both Landsat data using AVIRIS endmember bundles and the Landsat endmember bundles place the AVIRIS values within the error estimate, with the exception of several points that do not agree well for any of the cover types.

There is a BRDF effect associated with the view angle of AVIRIS relative to the sun with this flight line, which is 48.3° off of the solar azimuth. Spectra in the endmember bundles were located in the AVIRIS scene to ensure that they came from throughout the image rather than one side or the other. With the use of endmember bundles to encompass the variability of the image endmembers more effectively, the BRDF biases are better represented in the bundles. Fraction images do not show a bias to one side of the image or the other indicating that BRDF effect resulting from the flightline-sun relationship is minimal, see figure 4.11.

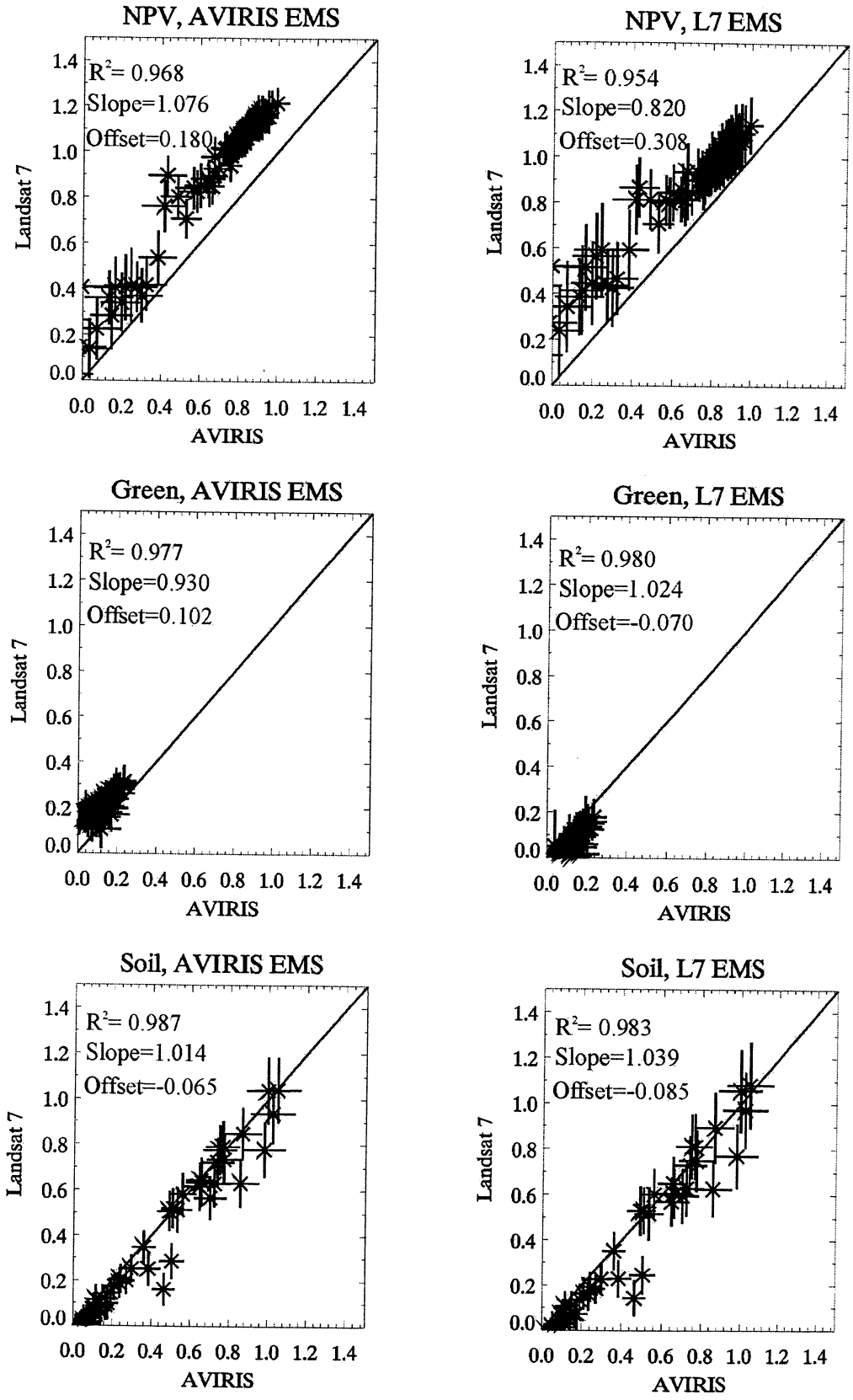

Figure 4.10. Logan cover fractions derived with AutoSMA.

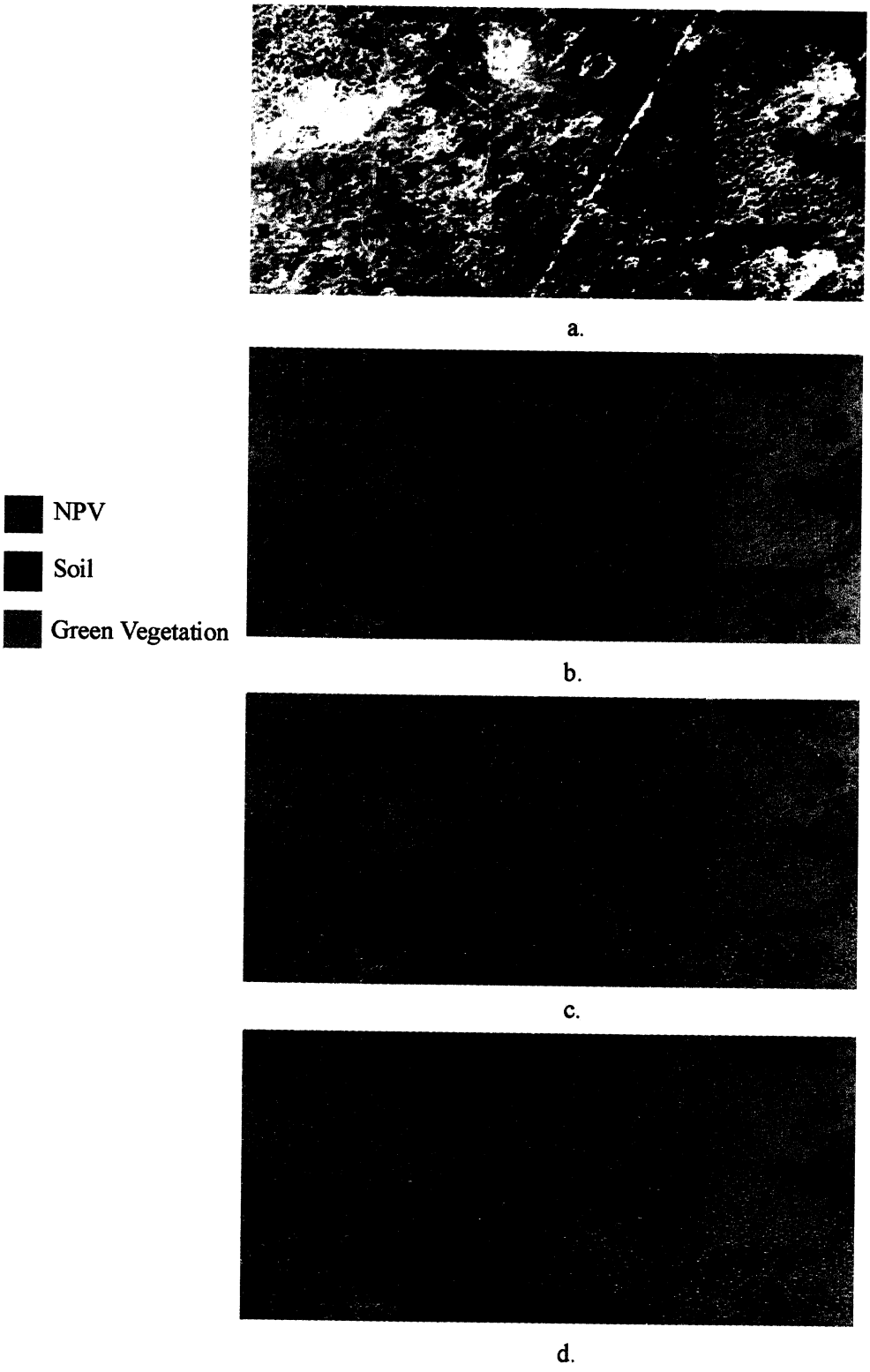

Figure 4.11. Logan fraction images all images have been stretched with a 2% stretch. a. CIR Logan AVIRIS sub-scene, b. AVIRIS fractions, c. Landsat 7 fractions derived with AVIRIS endmembers d. Landsat 7 endmember fractions.

The high correlation of NPV (figure 4.10) with this scene and relatively low standard deviation in comparison to the Ft. Morgan data is the result, most likely, of the quality of the endmembers. The vegetation cover that was observed during fieldwork was very thick in regions not covered with active dunes. The vegetation that was still standing was mostly senesced grass and there was a good cover of dead litter on the soil. There was soil showing through, but the vegetation cover from visual estimates was 80-90%. The NPV endmember pixels are mixtures of different types of litter, but this vegetation type is found throughout the image; essentially, the pixels are more solidly covered by litter than in the other images, resulting in purer pixels in the bundles.

Chapter 5

Discussion and Conclusions

Discussion

Field Method Problems

A 100m by 100m area for vegetation transects is not sufficient for the type of comparison used in this study and the counting methods were flawed. The Ft. Morgan site was generally uniform with a cottonwood in one area and some bare soil in another area being the main source of deviation from mixed vegetation cover. With the accuracy of georegistration being within a pixel and at worst 2 pixels, using only select pixels from a site that is 5 by 5 AVIRIS pixels, yields potential uncertainty. The PSF of both sensors requires an area that is larger than the total PSF be used. The size region used in this study is not large enough to select the center pixel of the study site and use that as a proxy for the region. Misregistration could put that pixel on the edge of the site boundary or beyond. If this study were to be performed again, several 1km by 1km areas should be used. This size region allows for more room for error in misregistration and the sensor PSF effects.

The counting in both sites was performed by two people with no noticeable bias in the counting method since no largely dissimilar numbers for visually similar cover were obtained. The counting method was flawed in its relation to remote sensing. If a shrub or bush intercepted the line it was counted as green vegetation, but the woody branches and senesced tissue and soil that were also showing beneath were not counted in the appropriate group. The counting was performed with an eolian description of ground cover. Interstitial spaces in the canopy revealed areas of bare soil and understory litter. From an eolian deposition stand point, the shrub or bush is providing 100% cover for the part of the ground it covers. Remotely sensed fractions reflect branches that can be seen with a "birds eye view" and soil and litter can be detected in this manner as well even though the surface is covered. A better method for assessing fractional cover in the field would involve very fine resolution counting (counting the cover type at every centimeter) and using a larger area. By using a larger area, edge effects are minimized, georegistration errors of the imagery are not as noticeable in a larger area, and the PSF of the sensor is better taken into consideration.

Unmixing Results

Physically infeasible fractions were found predominantly in the Logan scene and in a few regions in the Ft. Morgan line. Some cover fractions have large standard deviations, limiting their utility in quantifying vegetation and NPV differences. The reasons for these discrepancies can be associated with endmember availability and selection. In a 20m or 30m pixel, there is no "pure" cover, but a mixture of soil, NPV, green vegetation, and shade that comprises the "pure" pixel. A dominant cover

type has a greater effect on the recorded signal, but the overall signal is a mixture of the different species of that cover type. Landsat 7 pixels are minimally 40m by 40m with the sensor PSF compared with AVIRIS pixels of approximately 22.5m for Ft Morgan and 20.7m for Logan with AVIRIS' PSF. The sensors are inherently observing different regions on the ground no matter how well the images are georegistrered or spatially resampled to match.

The fractions that were computed in this study were not always physically feasible. Physically unreasonable mixtures are mathematically feasible. If the pixel being unmixed does not fit the mixing model of the endmembers a fraction greater than one or less than zero is the result; the pixel being unmixing is beyond the bounds of the endmember simplex. One of flaws with using user defined endmember bundles is these bundles can have spectra added to them or removed to make the mixture analysis produce more feasible results. The bundles can have spectra added or removed to reflect a desired response, with time there is always a better bundle to be gleaned from the data. Methods that implement broad field spectral libraries, such as the ones used by Asner and Lobell (2000) and Lobell et al (in review), can be used on multiple images regardless of date and time. The use of spectral databases appears to be the best objective method with finding endmembers and applying them in the appropriate combinations. This method of using a large spectral data base is currently only being applied to AVIRIS data, but perhaps in future studies, can be applied to multispectral data.

Image derived endmembers, while they are readily available and can characterize plant canopies more thoroughly, are subject to intense processing when

selecting the spectra to be placed into the bundle. The cut-off point of whether a pixel is pure enough to be included in a bundle is fuzzy when using image endmembers. Field and reference endmembers, when collected carefully, are pure spectra. Image endmembers are never completely pure due to surface cover, atmospheric artifacts and atmospheric modeling errors in the imagery, topography, and artifacts in the data. While never pure reference and field collected endmember spectra suffer by difficulty in reproducing solar geometry near the time of the overflight, which can significantly affect the resulting spectrum. Which type of endmembers produce better results is subjective based on the data collected.

The AVIRIS and Landsat 7 derived soil fractions provided good correlation with the minimum standard deviation. This is useful in observing the differences in the two sensors as well as adding spectral leverage to the Landsat 7 data. On the other hand, the large standard deviation using Landsat 7 endmembers (though well correlated) provides a cover estimate that includes the AVIRIS values. The standard deviation for the soil fractions derived with Landsat 7 are large enough that searching for fractional cover under 30% would have to include cover of upwards of 60% in some cases to include the error estimate. NDVI, though susceptible to soil color differences can be correlated to fractional cover and without the intensive user time and user biased procedure to select image endmembers.

In the context of a multi-year and multi-temporal study, such as the one undertaken by CSES to determine climatological impacts on the High Plains over a 15 year period, techniques such as using one group of endmembers for the entire study area are not feasible. No field data exists to meet the temporal needs of this

study regarding vegetation cover during the time span of this study (1985-2000) to calibrate the findings. The time period these images were collected ranges from June to October in a given year. By using one set of endmembers, one can observe how the scene has changed from those endmembers, but does not account for natural changes in phenology and plant succession; the fractional plant cover may be the same, but the change in fractions is related to the endmembers. To apply mixture analysis to a multi-year study such as CSES' High Plains climate study, there would need to be other constraints than relating to two near-simultaneous scenes. On a large-scale multi-year project without a basis of comparison, such as AVIRIS lines or historical field measurements, image derived endmembers introduce error. There is simply too much uncertainty in the temporal coverage of the images to extract endmembers that are going to correspond throughout the length of the study to use a single set of endmember bundles for an entire set of images.

Image derived fractions of cover below 30% correlated well between the two sensors, though the fractions were not consistently overestimated or underestimated for any of the cover types. Fractions of soil greater than 70% were found in the regions of interest in FM0210 and the Logan scene which included spurious fractions that indicated the spectra had not been sufficiently modeled in the endmember bundles. The AVIRIS soil fractions for all scenes are well correlated with the Landsat 7 fraction even though Landsat 7 values are offset (do not correlate one to one with the AVIRIS fractions), with the presence of AVIRIS data they can be modeled to determine a more likely fraction.

Conclusions

Near-simultaneous overflights of two different sensors provide an excellent means of comparing results and removing some unknowns. The high correlation between all the AVIRIS scenes used and the corresponding areas in the Landsat 7 images indicate that Landsat data can be unmixed to show fractions of soil, NPV and green vegetation and be related to the AVIRIS data when the appropriate endmembers are used. Unmixing with Landsat endmembers alone does correlate well with the AVIRIS results but with the fractions having a relatively larger margin of error. Fraction images produced by AutoSMA correlate well to visual interpretation of the imagery indicating that this technique can be used for qualitative mapping. Combining the endmember bundles from FM0209 and FM0210, which are on the same soil type, and achieving similar soil fractions shows that if the appropriate soil bundle is chosen, then the NPV and green vegetation bundles are not as significant if one is seeking to map soil fractions.

The goal of this thesis is to determine how well Landsat data can map fractional cover of vegetation on the High Plains. The desired results can be inverted to mapping fraction of bare soil since it is the amount of exposed soil that is the factor in dune reactivation. A linear spectral mixture analysis approach using endmember bundles was used to arrive at sub-pixel fractional cover for both AVIRIS and Landsat 7 images. Fractional cover was mapped in two semi-arid environments with a smaller error estimate achieved using AVIRIS endmembers to unmix Landsat 7 data. Landsat 7 fractions derived with Landsat 7 endmembers are well correlated with the AVIRIS derived cover fractions for all scenes, but have large error estimates. These large

standard deviations, but high correlation coefficients, indicate that Landsat endmembers can be used to delineate between soil and NPV but without the certainty of using AVIRIS endmember bundles. Soil fractions using AVIRIS endmembers are always highly correlated and have a smaller standard deviation than that fractions produced with Landsat 7 image endmembers.

Appendix A

FM0209 AVIRIS fractions and standard deviations

ROI's	npv	green	soil	sum	npv	green	soil
1	0.377861	0.186089	0.461609	1.025559	0.131963	0.101239	0.069321
2	0.397039	0.173672	0.456539	1.02725	0.138884	0.09855	0.078608
3	0.503654	0.187133	0.292117	0.982904	0.142697	0.105643	0.083313
4	0.378423	0.160392	0.476592	1.015407	0.137012	0.095333	0.076159
5	0.335811	0.151156	0.552159	1.039126	0.130883	0.092329	0.070435
6	0.435909	0.096797	0.48222	1.014926	0.113457	0.084289	0.072374
7	0.435405	0.202141	0.386101	1.023647	0.14369	0.110078	0.077177
8	0.348569	0.263392	0.440634	1.052595	0.154173	0.120311	0.076153
9	0.427172	0.091587	0.505079	1.023838	0.106131	0.085457	0.065738
10	0.47465	0.067762	0.427446	0.969858	0.119855	0.077112	0.0819
11	0.454118	0.15547	0.392934	1.002522	0.132375	0.09994	0.078976
12	0.469024	0.021066	0.494086	0.984176	0.110094	0.069238	0.079242
13	0.45141	0.141398	0.387555	0.980363	0.130688	0.090988	0.07972
14	0.400242	0.268635	0.34095	1.009827	0.16016	0.122724	0.081766
15	0.356332	0.246642	0.419147	1.022121	0.152561	0.113818	0.078933
16	0.479462	0.254772	0.259424	0.993658	0.157518	0.120446	0.084343
17	0.378932	0.215007	0.426097	1.020036	0.142172	0.107566	0.076281
18	0.497442	0.243288	0.247317	0.988047	0.158406	0.121259	0.087995
19	0.51183	0.146483	0.362776	1.021089	0.124387	0.102475	0.073507
20	0.396832	0.198078	0.421837	1.016747	0.139542	0.102944	0.078167
21	0.432504	0.066121	0.511115	1.00974	0.110676	0.077396	0.072255
22	0.456066	0.309839	0.166097	0.932002	0.177754	0.133321	0.098717
23	0.476729	0.065975	0.430337	0.973041	0.1047	0.076953	0.074681
24	0.489368	0.016001	0.459334	0.964703	0.102359	0.070286	0.077232
25	0.461396	0.0653	0.45161	0.978306	0.111143	0.08109	0.07434
26	0.490384	0.097521	0.356762	0.944667	0.120629	0.08306	0.081786
27	0.305841	0.229786	0.47692	1.012547	0.14841	0.107177	0.074477
28	0.421414	0.052996	0.504452	0.978862	0.10562	0.076562	0.069112
29	0.387816	0.162844	0.439247	0.989907	0.131675	0.099177	0.07282
30	0.479523	0.131392	0.349482	0.960397	0.129501	0.088725	0.083719
31	0.280483	0.286271	0.442217	1.008971	0.161366	0.118738	0.076777
32	0.578397	0.254828	0.11694	0.950165	0.16085	0.12596	0.090167
33	0.50453	0.227139	0.232438	0.964107	0.165782	0.115875	0.093772
34	0.362613	0.284229	0.327849	0.974691	0.164572	0.124844	0.085204
35	0.278526	0.415477	0.186793	0.880796	0.206112	0.151012	0.099886

FM0209 Landsat 7 fractions and standard deviations with AVIRIS endmembers

ROI's	npv	green	soil	sum	npv	green	soil
1	0.322355	0.147921	0.549879	1.020155	0.165326	0.097772	0.096685
2	0.343333	0.148638	0.525475	1.017446	0.174966	0.100984	0.103942
3	0.418255	0.155582	0.404505	0.978342	0.223434	0.119039	0.127792
4	0.336034	0.129886	0.550125	1.016045	0.180717	0.100957	0.103163
5	0.298735	0.100923	0.634187	1.033845	0.158185	0.093238	0.090084
6	0.377792	0.035931	0.590317	1.00404	0.163686	0.085108	0.102996
7	0.328566	0.189207	0.511161	1.028934	0.16668	0.105767	0.093211
8	0.321729	0.190095	0.531309	1.043133	0.181399	0.115114	0.094233
9	0.373847	0.055465	0.596908	1.02622	0.142416	0.087169	0.089514
10	0.392978	0.070227	0.502978	0.966183	0.223701	0.102052	0.132855
11	0.381995	0.182895	0.430635	0.995525	0.229408	0.130529	0.127007
12	0.415207	0.009771	0.558497	0.983475	0.183242	0.086326	0.116809
13	0.371399	0.114234	0.480703	0.966336	0.218178	0.105458	0.125199
14	0.325177	0.217682	0.453343	0.996202	0.193143	0.11743	0.104748
15	0.306427	0.190785	0.512386	1.009598	0.172354	0.108208	0.091564
16	0.416287	0.199872	0.364133	0.980292	0.231472	0.125517	0.133449
17	0.326569	0.174247	0.518352	1.019168	0.189331	0.114481	0.099056
18	0.372247	0.207418	0.398341	0.978006	0.245243	0.135226	0.135715
19	0.396074	0.131717	0.481302	1.009093	0.176487	0.101729	0.103199
20	0.307311	0.164043	0.540627	1.011981	0.18044	0.106837	0.09824
21	0.350485	0.055684	0.604339	1.010508	0.152218	0.090295	0.088251
22	0.391622	0.241617	0.312111	0.94535	0.287325	0.157448	0.151924
23	0.371934	0.069161	0.537048	0.978143	0.191817	0.094958	0.114213
24	0.416514	0.013184	0.54098	0.970678	0.179712	0.086904	0.113114
25	0.377482	0.057184	0.533288	0.967954	0.176467	0.091152	0.108787
26	0.40923	0.082343	0.441285	0.932858	0.2188	0.103402	0.127191
27	0.252494	0.165373	0.591443	1.00931	0.154601	0.098387	0.084525
28	0.381941	0.035556	0.559312	0.976809	0.165671	0.089762	0.098746
29	0.357813	0.098535	0.525867	0.982215	0.195412	0.107208	0.106743
30	0.373484	0.132771	0.449656	0.955911	0.230649	0.119585	0.126776
31	0.287675	0.246371	0.472863	1.006909	0.186935	0.12034	0.096634
32	0.485485	0.224654	0.227147	0.937286	0.289192	0.1553	0.162777
33	0.437985	0.184625	0.329068	0.951678	0.290621	0.147387	0.161796
34	0.308682	0.242661	0.425897	0.97724	0.217879	0.134426	0.10874
35	0.252211	0.379732	0.286846	0.918789	0.274591	0.175591	0.138644

FM0209 Landsat 7 fractions and standard deviations with Landsat 7 endmembers

ROI's	npv	green	soil	sum	npv	green	soil
1	0.266657	0.166378	0.61989	1.052925	0.177973	0.049122	0.137783
2	0.268977	0.173021	0.609581	1.051579	0.19409	0.050555	0.149449
3	0.275934	0.200787	0.536739	1.01346	0.254188	0.055633	0.194133
4	0.270492	0.154245	0.622317	1.047054	0.204628	0.054689	0.157997
5	0.265616	0.118417	0.675765	1.059798	0.188123	0.056019	0.146588
6	0.289088	0.082906	0.655621	1.027615	0.198244	0.055571	0.153789
7	0.257675	0.205925	0.597283	1.060883	0.170184	0.046072	0.132241
8	0.265414	0.203983	0.602507	1.071904	0.191948	0.054624	0.149112
9	0.282385	0.101225	0.660809	1.044419	0.173377	0.052557	0.137639
10	0.28568	0.115731	0.599447	1.000858	0.252439	0.06006	0.18995
11	0.268385	0.212516	0.549817	1.030718	0.251253	0.058216	0.193187
12	0.295546	0.069926	0.642162	1.007634	0.215026	0.056376	0.164086
13	0.273415	0.150433	0.578366	1.002214	0.244628	0.057381	0.184228
14	0.253131	0.228117	0.549543	1.030791	0.201705	0.049178	0.156142
15	0.253269	0.201625	0.582986	1.03788	0.185778	0.05188	0.144472
16	0.27339	0.236979	0.510669	1.021038	0.267564	0.053001	0.204944
17	0.261456	0.192296	0.592199	1.045951	0.214595	0.059017	0.165816
18	0.266391	0.229155	0.523424	1.01897	0.269961	0.058997	0.206155
19	0.280855	0.17361	0.581174	1.035639	0.196369	0.050857	0.152561
20	0.254735	0.177625	0.610932	1.043292	0.204258	0.055153	0.157079
21	0.273729	0.095653	0.658825	1.028207	0.197748	0.058817	0.154778
22	0.257109	0.266616	0.463227	0.986952	0.320221	0.067387	0.243797
23	0.287616	0.108438	0.609871	1.005925	0.222233	0.057288	0.171331
24	0.293294	0.074545	0.625111	0.99295	0.213144	0.05669	0.16375
25	0.281344	0.102424	0.61042	0.994188	0.208794	0.05571	0.16148
26	0.2816	0.133255	0.547903	0.962758	0.249688	0.057811	0.1902
27	0.241589	0.164642	0.633636	1.039867	0.179724	0.053181	0.139271
28	0.284509	0.085424	0.6248	0.994733	0.203596	0.058836	0.159355
29	0.282109	0.131862	0.590188	1.004159	0.217755	0.062044	0.168403
30	0.252909	0.172076	0.563746	0.988731	0.277995	0.064868	0.214929
31	0.242726	0.243859	0.555643	1.042228	0.189556	0.049258	0.146612
32	0.274958	0.278754	0.424694	0.978406	0.363048	0.069681	0.277798
33	0.277835	0.227775	0.489287	0.994897	0.342403	0.068469	0.25937
34	0.248604	0.245569	0.514312	1.008485	0.224732	0.058085	0.174362
35	0.205019	0.347141	0.415985	0.968145	0.290256	0.060257	0.223238